

# Study Hubble constant anisotropies with the Zwicky Transient Facility

SARASAR Antoine  
Supervisor: Ph.D Philipe Rosnet

September 9, 2023

## Abstract

We propose to study the anisotropies of the Hubble constant with simulations of type Ia supernovae (SNe Ia) as observed by ZTF. We have partitioned the sky using two methods: one allowing fixed patches of the sky and the other based on the distribution of SNe Ia. We performed a first analysis without anisotropy to test the sensitivity of the ZTF typical data sample. We then introduced a dipole effect into the simulations, with the redshift following the dipole's tilt. This dipole is found again in the analysis, showing that ZTF can be sensitive to an anisotropy effect.

---

## Contents

<b>List of Figures</b>	<b>2</b>
<b>Acknowledgement</b>	<b>3</b>
<b>Introduction</b>	<b>4</b>
<b>I Supernovae Type Ia Cosmology</b>	<b>4</b>
A Standard Cosmology . . . . .	4
A.1 Cosmological Principle . . . . .	4
A.2 Friedmann-Lemaître-Robertson-Walker metric - Metric of the Universe . . . . .	5
A.3 $\Lambda$ CDM Model . . . . .	6
A.4 Beyond $\Lambda$ CDM . . . . .	7
A.5 Luminosity Distance . . . . .	7
B Supernova . . . . .	9
B.1 Classification . . . . .	9
B.2 Type Ia Supernovae . . . . .	9
B.3 SNe Ia Standardization . . . . .	9
C Hubble Tension . . . . .	10
<b>II The Zwicky Transient Facility</b>	<b>11</b>
A Architecture . . . . .	11
B Survey Strategy . . . . .	12
<b>III Simulations</b>	<b>13</b>
A <code>simsurvey</code> . . . . .	13
B Supernova selection . . . . .	13

<b>IV Anisotropies Analysis</b>	<b>16</b>
A Hubble Diagram . . . . .	16
B Partitionning . . . . .	17
B.1 HEALPix . . . . .	17
B.2 HEALPix Method . . . . .	19
B.3 Clustering Algorithm . . . . .	19
C $H_0$ Variations . . . . .	20
C.1 Method . . . . .	21
C.2 Analysis with HEALPix Patch . . . . .	21
C.3 Analysis with Clustering Patch . . . . .	22
C.4 Comparison . . . . .	23
D Dipole Introduction . . . . .	23
D.1 Dipole Effect . . . . .	23
D.2 Analysis with the two Partitioning Methods . . . . .	24
D.3 Reverse Fit . . . . .	25
<b>Conclusion</b>	<b>28</b>
<b>References</b>	<b>29</b>
<b>Appendix</b>	<b>30</b>
A Appendix 1 . . . . .	30
B Appendix 2 . . . . .	30
C Appendix 3 . . . . .	31
D Appendix 4 . . . . .	32

## List of Figures

1 CMB and SDSS Galaxy Map . . . . .	5
2 An example of a Hubble Diagram . . . . .	8
3 Stretch and color correlation with the magnitude . . . . .	10
4 Hubble Tension comparison plot . . . . .	11
5 Sky coverage and number of observation epochs for DR17 . . . . .	12
6 BTS spectroscopic selection . . . . .	14
7 Light curves . . . . .	15
8 Sky map of SNe Ia selected according to their redshift . . . . .	15
9 Hubble Diagram . . . . .	17
10 Orthographic view of HEALPix partition of the sphere . . . . .	18
11 Pixel representation of the SNe Ia distribution on equatorial coordinate . . . . .	18
12 Distribution per patch . . . . .	19
13 Elbow method . . . . .	20
14 Distribution per patch . . . . .	20
15 $H_0$ variations for HEALPix method . . . . .	21
16 Hubble Diagrams for specific patch . . . . .	22
17 $H_0$ variations for clustering method . . . . .	22
18 Comparison between HEALPix and clustering method . . . . .	23
19 Dipole anisotropy effect Map . . . . .	24
20 Sky map for dipole . . . . .	24
21 $H_0$ value for dipole effect . . . . .	25
22 Dipole anisotropy map with fitted directions . . . . .	25
23 Distributions of the difference between fitted dipole and input dipole . . . . .	26
24 Reverse Fit for different dipoles with clustering method . . . . .	27
25 Polygon map . . . . .	30
26 Reverse Fit for different dipoles with HEALPix method . . . . .	32

## Acknowledgement

I would like to thank all the people who contributed to the success of my internship and the writing of this report.

First of all, I would like to thank my internship supervisor, Dr. **Philippe ROSNET**, teacher-researcher, for having accepted my internship and his wise and enlightened advice.

I would also like to thank all the people who helped me directly on this subject, such as Dr. **Marie AUBERT**, a postdoc, for her idea of using clustering. Likewise, I would like to thank Dr. **Philippe GRIS**, researcher, for his advice in Python.

Thanks to Dr. **Nicoleta PAUNA**, teacher-researcher, for organizing basketball sessions to clear the mind.

I would also like to thank Dr. **Johan COHEN-TANUGI**, researcher, for his fostering in the office.

The help of other trainees like **Andrea ANTONIALI** or **Morvan VINCENT** was a great support.

I must also say thank you to all the other people in the Cosmology group with whom I had less interaction but who welcomed me pleasantly into the group.

Finally, I would like to thank the Laboratoire de Physique de Clermont for welcoming me to its premises.

## Introduction

Current Cosmology is essentially founded on the cosmological principle that the Universe is isotropic and homogeneous. Today several studies show hints of contradiction with this principle. As said by Steven Weinberg, American physicist: “*The real reason for our adherence to the cosmological principle is not that it is surely correct, but rather, that it allows us to make use of the extremely limited data provides to cosmology by observational astronomy*”, for him this attachment to this principle comes from the lack of data. The number of data only increasing, thanks to technological progress and the advancement of new approaches, we observe some contradictions. One of these contradictions is the Hubble tension. Indeed, the value of the Hubble constant  $H_0$  (current value of the Hubble parameter which represents the rate of the cosmic expansion) is subject to debate. There is today a difference of about  $5 \text{ km s}^{-1} \text{ Mpc}^{-1}$  on the value of this constant when it is determined from the cosmic microwave background with the standard model of cosmology or when it is obtained by direct measurement using the observation of type Ia supernovae.

Many studies focus on these differences in value obtained and thus look for anisotropies in the cosmic expansion. Studies like [1], [2] and [3] feed the motivation of this internship topic. The goal of this topic is to study the sensitivity to detect anisotropies of the Hubble constant with the Zwicky Transient Facility (ZTF), an astronomical survey located at Mount Palomar (California, United States). ZTF is an excellent machine for detecting transient objects such as supernovae Ia (SNe Ia). This study will use realistic ZTF simulation of SNe Ia to develop an analysis of differential measurement of  $H_0$  as a function of the sky direction. The goal is to quantify the sensitivity of the measurement to potential anisotropies.

We will start with a first part about supernovae cosmology. Then we will give a brief description of ZTF and simulations. Finally we will describe the methods used in our study and the analysis of the results obtained.

## I Supernovae Type Ia Cosmology

### A Standard Cosmology

This part is inspired by [4], [5] as well as on the Master 2 Cosmology lecture of Philippe Rosset. We will see in section A.1 the cosmological principle and what it implies, in section A.2 we will talk about general relativity and the FLRW metric, in section A.3 we will explain the  $\Lambda$ CDM model, in A.4 we will see models beyond the  $\Lambda$ CDM and finally in section A.5 we will talk about the luminosity distance.

#### A.1 Cosmological Principle

Modern Cosmology is based on the cosmological principle (CP), most models and observations are based on this principle. The CP states that the Universe is a four-dimensional space-time, spatially homogeneous and isotropic at large scale, i.e. it is the same in all directions and at any point. The Universe is therefore invariant by translation and rotation. This principle has received several confirmations such as the quasi-isotropy of the cosmic microwave background (CMB) (left panel **Fig.1**). However, surveys such as the Sloan Digital Sky Survey (SDSS)<sup>1</sup> have revealed that the CP was no longer respected at small scales ( $<100 \text{ Mpc}$ ) as can be seen on the right panel of **Fig.1**.

We will see in chapter II, that the ZTF survey works at low redshift, i.e. in the Nearby Universe, which will allow the study of local anisotropies.

<sup>1</sup> <https://www.sdss.org>

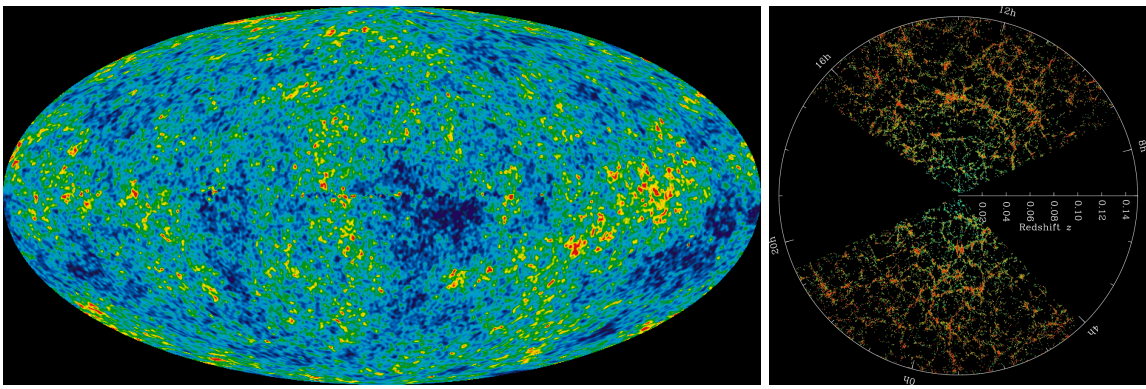


**Figure 1:** CMB and SDSS Galaxy Map. Left panel: temperature anisotropy map of the CMB from [6], this electromagnetic radiation is very homogeneous; Right panel: Map distribution of the galaxies in the nearby Universe from [7], each point corresponds to a galaxy and the colors represent the age of the stars, dark parts are due to the dust of the Milky Way.

## A.2 Friedmann-Lemaître-Robertson-Walker metric - Metric of the Universe

The fundamental point of the current Cosmology is based on the general relativity stated by Albert Einstein, more precisely on his equation of fields which connect the geometry of the space time ( $g_{\mu\nu}$ ) and its energy content ( $T_{\mu\nu}$ ) as we can see it with the following equation:

$$R_{\mu\nu} - \frac{1}{2}g_{\mu\nu}R + \Lambda g_{\mu\nu} = -\frac{8\pi G}{c^4}T_{\mu\nu} \quad (\text{I.1})$$

where  $R_{\mu\nu}$  is the Ricci Tensor,  $g_{\mu\nu}$  is a metric tensor,  $R$  is the scalar curvature,  $\Lambda$  is the cosmological constant introduced by A. Einstein to obtain a static Universe at large scale and it is expressed in  $\text{m}^{-2}$ ,  $T_{\mu\nu}$  the energy-momentum tensor expressed in  $\text{J m}^{-3}$ ,  $G$  Newton's gravitational constant<sup>2</sup>,  $c$  the speed of light<sup>3</sup>.

We can then build the metric that takes into account the homogeneity and isotropy stated by the CP, it is the Friedmann-Lemaître-Robertson-Walker (FLRW) metric. It is constructed from the relativistic invariant  $ds^2$  expressed in terms of the metric tensor  $g_{\mu\nu}$  as follows:

$$ds^2 = g_{\mu\nu}dx^\mu dx^\nu \quad (\text{I.2a})$$

$$= c^2dt^2 - a^2(t)\left(\frac{dr^2}{1-kr^2} + r^2d\Omega^2\right) \quad (\text{I.2b})$$

where  $a(t)$  is the Universe scale factor (a length),  $d\Omega^2 = d\theta^2 + \sin^2\theta d\phi^2$  with the comoving coordinates  $r, \theta, \phi$  and  $t$  are space-time coordinates and  $k$  indicates the curvature 1,-1 or 0 for a close, open and flat Universe. The metric can also be expressed with the radial comoving coordinate  $\chi$  as in equation I.3.

$$ds^2 = c^2dt^2 - a^2(t)(d\chi^2 + S_k^2(\chi)d\Omega^2) \quad (\text{I.3})$$

with

$$S_k(\chi) = \begin{cases} \sin(\chi) & \text{if } k = 1 \\ \chi & \text{if } k = 0 \\ \sinh(\chi) & \text{if } k = -1 \end{cases} \quad (\text{I.4})$$

By introducing the approximation that the energy distribution in the Universe corresponds to a perfect fluid, called cosmic fluid, we find two fundamental equations which are solutions of the components of

<sup>2</sup>  $G = 6.67384 \times 10^{-11} \text{ m}^3 \text{ kg}^{-1} \text{s}^{-2}$

<sup>3</sup>  $c = 3.00 \times 10^8 \text{ m s}^{-1}$

Einstein's field equations to describe the dynamics of the Universe. These equations are the first and second Friedmann-Lemaître (FL) equations (with  $c \equiv 1$ ):

$$H^2 = \left(\frac{\dot{a}}{a}\right)^2 = \frac{8\pi G}{3}\rho + \frac{\Lambda}{3} - \frac{k}{a^2} \quad (\text{I.5a})$$

$$2a\ddot{a} + \dot{a}^2 + k = -8\pi G P a^2 + \Lambda a^2 \quad (\text{I.5b})$$

where  $H$  is the Hubble parameter,  $\rho$  is the energy density and  $P$  is the pressure of the cosmic fluid. This density and the pressure can be related by the general equation of state for a fluid as follows:

$$P = \omega\rho \quad (\text{I.6})$$

where  $\omega$  is usually a constant parameter. With these equations we can also find the conservation equation:

$$\dot{\rho} + 3\frac{\dot{a}}{a}(\rho + P) = 0 \quad (\text{I.7})$$

With all the equations seen in this part we can explain the energy content of the universe as well as the implementation of model as the  $\Lambda$ CDM model that we will see in the following part [A.3](#)

### A.3 $\Lambda$ CDM Model

In the universe we find non-relativistic matter: baryonic matter (the ordinary matter we know) and cold dark matter (CDM). This matter is called cold because it moves slowly compared to the speed of light and it is dark because it interacts weakly with other matter and electromagnetic radiation. This matter was introduced following the observations of Vera Rubin (1968) and Zwicky (1933). The first having observed that the rotation curves of stars and gas clouds inside galaxies are more important at large radius than expected by known matter and the second observed that the total mass to bind the galaxies of the Coma cluster was two orders of magnitude higher than Hubble estimation. Our Universe is also composed of relativistic matter (or radiation), this matter are photons and neutrinos, particles that move almost at the speed of light. Observations have shown that the Universe is in accelerated expansion, property which can not be explained with a Universe composed only of non-relativistic matter and radiation. It is then introduced the dark energy that is a fluid with a negative pressure.

Thanks to the equations seen in the previous part we can define the mass density for each component of the Universe. For the dark energy we associate it with the cosmological constant which is considered as a fluid with energy (mass) density:

$$\rho_\Lambda = \frac{\Lambda}{8\pi G} \quad (\text{I.8})$$

The first FL equation [\(I.5a\)](#) then becomes:

$$\frac{8\pi G}{3}a^2(\rho_r + \rho_m + \rho_\Lambda - \rho_c) = k \quad (\text{I.9})$$

where  $\rho_c$  is the critical mass density defined as:

$$\rho_c = \frac{3H^2}{8\pi G} \quad (\text{I.10})$$

We use the critical mass density because it is convenient to express all densities with respect to  $\rho_c$ . With the equation [I.9](#) we can deduce the Budget equation of the Universe:

$$\Omega_{tot} = \Omega_r + \Omega_m + \Omega_\Lambda = 1 - \Omega_k \quad (\text{I.11})$$

where  $\Omega_i = \frac{\rho_i}{\rho_c}$  with  $i = (r, m, \Lambda)$  and  $\Omega_k = -\frac{k}{a^2 H^2}$ , are density cosmological parameters. Finally from equation [I.5a](#) we find the following Hubble parameter expression:

$$H(a) = H_0 \sqrt{\frac{\Omega_{r,0}}{a^4} + \frac{\Omega_{m,0}}{a^3} + \Omega_{\Lambda,0} + \frac{\Omega_{k,0}}{a^2}} \quad (\text{I.12})$$

where zeros refer to  $t_0$  as the current cosmic time.

The  $\Lambda$ CDM model where the late Universe is dominated by dark energy of the form of the cosmological constant ( $\Lambda$ ) and the non-relativistic matter (CDM). In  $\Lambda$ CDM,  $\Omega_k = 0$ , so the equation I.12 becomes:

$$H(a) = H_0 \sqrt{\frac{\Omega_{m,0}}{a^3} + \Omega_{\Lambda,0}} \quad (\text{I.13})$$

#### A.4 Beyond $\Lambda$ CDM

The  $\Lambda$ CDM model is the most commonly used model, only some models try to go further like the  $\omega$ CDM model which is based on  $\Lambda$ CDM. In  $\omega$ CDM we replace the cosmological constant by a dark energy density. Chevallier and Polarski are realized the following parametrisation in  $\omega$ CDM:

$$\omega(a) = \omega_0 + w_a(1 - a) \quad (\text{I.14})$$

where  $\omega$  is the dark energy state parameter,  $\omega_0$  is the current value of  $\omega$  and  $w_a$  is the directing coefficient that determines the temporal dependency. With this model we arrive at the following distribution:  $\Omega_m \approx 0.3$  and  $\Omega_{DE} \approx 0.7$ .

Within the  $\Lambda$ CDM model there are tensions such as the Hubble tension which we will describe in part C. To adjust this tension many models based on the FLRW framework have been proposed but none is satisfactory. An emerging idea is that there would be a violation of the cosmological principle because the CP does not pass all the observational tests and it is what [3] proposes to study. They decide to position themselves within the framework of a dipolar cosmology because it is the simplest case that can accommodate a cosmic flow and which generalizes FLRW. For this to build their metric of dipolar cosmology they assume homogeneity and axisymmetry, all the parameters then depend on time. They also introduce a parameter that parametrizes the anisotropy. Moreover, this metric is constructed in such a way that the redshift is chosen to be along the cosmic flow, i.e. along a tilt. They study models involving a fluid of constant equation of state and a cosmological constant. Their analysis, based on the Einstein field equation taking into account a tilt of the energy-momentum tensor of the cosmic fluid, shows the instability of FLRW cosmology in the face of tilt disturbances. This tilt, contrary to the cosmic shear which quickly fades as shown by the Cosmic No-Hair Theorems – the fact that the cosmic acceleration erases the anisotropies – remains important or even increases with an expanding Universe. Even if the results obtained by [3] do not correspond to a realistic model, they show the theoretical possibility of an instability due to dipole disturbances. The most important point shown by [3] is the difference between tilt and shear.

#### A.5 Luminosity Distance

We have already talked about the fact that the Universe is expanding, so it is crucial to know the distances that separate us from extragalactic objects. For this there is Hubble's law which links the speed and distance of galaxies in the nearby Universe.

$$v = H_0 d \simeq cz \quad (\text{I.15})$$

We notice that this expansion is translated by a redshift  $z$ . The redshift accounts for the distance of an object because we notice a shift towards the long wavelengths of the spectral rays, it is defined as follows:

$$z = \frac{\lambda_O - \lambda_S}{\lambda_S} \quad (\text{I.16})$$

where  $\lambda_S$  is the emission wavelength and  $\lambda_O$  is the observed one. We can relate the redshift to the scale factor, and this redshift is called cosmological redshift:

$$z + 1 = \frac{\lambda_0}{\lambda} = \frac{a_0}{a} \quad (\text{I.17})$$

where  $a_0 = 1$  is the scale factor at the current cosmic time (by convention). We can then rewrite equation I.13 with the cosmological redshift:

$$H(z) = H_0 \sqrt{(1+z)^3 \Omega_m + \Omega_\Lambda} \quad (\text{I.18})$$

Another way to determine distances is to use luminosity. The flux is defined as:

$$F = \frac{L}{4\pi d_L^2} \quad (\text{I.19})$$

where  $F$  is the luminous flux received from the object expressed in  $\text{W m}^{-2}$ ,  $L$  the emitted luminosity expressed in  $\text{W}$  and  $d_L$  the luminosity distance expressed in  $\text{m}$  (in parsec in Cosmology). The expression of the distance of luminosity that we choose in this subject is taken from [8] for  $\Lambda\text{CDM}$  model and is expressed as follows:

$$d_L = \frac{(1+z)}{H_0} \int_0^z \frac{dz'}{\sqrt{((1+z')^3 - 1)\Omega_m + 1}} \quad (\text{I.20})$$

It is also common to use the distance modulus, the distance modulus is a measure of the distance of a celestial object, as seen from Earth, using its apparent magnitude and its absolute magnitude:

$$\mu = m - M \quad (\text{I.21})$$

where  $m$  is the apparent magnitude which measures the brightness of a celestial object, as perceived by an observer located on Earth. Brighter objects have lower apparent magnitude, while dimmer objects have higher apparent magnitude.  $M$  is the absolute magnitude – magnitude of a star if the star was at 10 pc – is a measure of an object's intrinsic brightness, that is, how much light it actually emits.

There is also a relation between the distance of luminosity and the distance modulus:

$$\mu = 5 \log_{10}(d_L(\text{Mpc})) + 25 \quad (\text{I.22})$$

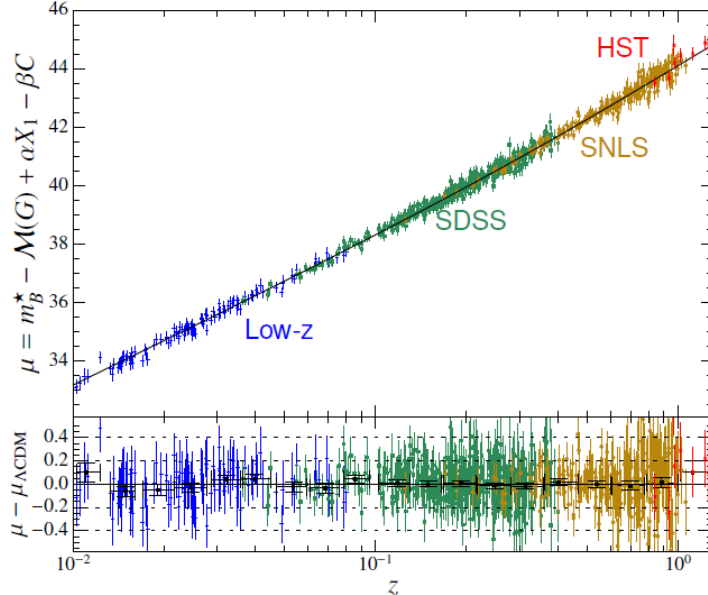


**Figure 2:** Hubble diagram from [9]. Top panel: Hubble diagram of a combined sample; Bottom panel: Residuals from the best-fit  $\Lambda\text{CDM}$  cosmology as a function of redshift.

The distance modulus allows to make a Hubble diagram which represents the distance modulus as a function of the redshift (see **Fig.2** for an example of an Hubble diagram). To built this kind of diagram we use distance modulus from standard candles like Cepheid<sup>4</sup> or Type Ia Supernovae (SNe Ia). A standard candle is an astronomical object that has a known luminosity. Most methods for determining distances in cosmology use these candles because they are easily observable and measurable. We will see in section **B**, SNe Ia properties and what their study brings.

## B Supernova

The determination of distances in cosmology is paramount, one of the most powerful tools is the type Ia supernovae. This is what we propose to see in this part inspired by [8], [4] and [5]. In section **B.1** we will define what is a supernova and how to classify them, then in section **B.2** we will talk about the properties of SNe Ia and finally in section **B.3** we will see the standardization and the Tripp relation.

### B.1 Classification

The term Supernova was first introduced by Baade and Zwicky, it refers to the result of the violent explosion of a star at the end of its life. This explosion is accompanied by an increase in luminosity over a short period followed by a slower decrease of luminosity, it is therefore a transient object.

We can classify these supernovae in subsets characterized by the properties of the observed supernovae. We can classify supernovae according to their spectrum, the first classification is done on the presence of hydrogen in the spectrum. Type I supernovae have no hydrogen in their spectrum and the type II have presence of hydrogen in their spectrum. Type I supernovae are divided into subclasses, for example when there is a massive presence of silicon, calcium, sulfur and iron we say that the supernovae are of type Ia, and if there is a massive presence of helium and no silicon it is SNe Ib, when there is neither helium nor silicon it is SNe Ic. We can also make other subset for type II but is not the subject of this topic. Note that other classification criteria exist. There are two mechanisms that give rise to supernovae. Firstly the thermonuclear explosion of white dwarf which gives rise to SNe Ia and secondly the supernovae with core collapse of a massive star representing all other supernovae.

Supernovae are very rare events, to measure their rarity we can talk about explosion rate expressed in  $\text{Mpc}^{-3} \text{year}^{-1}$ . For example the number of supernovae observed in our galaxy, the Milky Way, in the last millennium is counted in units. In [8] they give a local rate of SNe Ia of about  $3 \times 10^{-5} \text{ Mpc}^{-3} \text{year}^{-1}$ .

### B.2 Type Ia Supernovae

One of the methods to determine the Hubble constant  $H_0$ , is the standard candle method, where we assume a homogeneous luminosity for SNe Ia. We then use the observed luminosity to deduce the distance. This method is used because SNe Ia can become much brighter than their host galaxies at their peak luminosity. Usually we use the *B*-band (blue) for their luminosity, in this band the maximum luminosity is reached in about fifteen days. SNe Ia are excellent probes for measuring extragalactic distances thanks to the homogeneity of their luminosity because they have a low dispersion in luminosity. Their light curve, which represents the flux as a function of time, are perfectly observable. The accelerating expansion of the current Universe was established with SNe Ia, and those standard candle remains the most powerfull distance indicators thanks to their standardization.

### B.3 SNe Ia Standardization

SNe Ia are not exactly standard candles, but they can be standardized. This standardization is done thanks to the intrinsic luminosity of SNe Ia and their light curve which are associated with sources of

---

<sup>4</sup> Variable stars with high luminosity  $L_{\text{cepheid}} = (1 - 10) \times 10^3 L_\odot$

variability established from the data. This standardization reduces the dispersion in magnitude of the SNe Ia. The most commonly used relation to measure distances is the Tripp relation which defines the distance modulus as:

$$\mu = m_B^* - M_B + \alpha x_1 - \beta c \quad (\text{I.23})$$

where  $m_B^*$  is the observed maximum  $B$ -band magnitude,  $M_B$  is the absolute magnitude of the SNe Ia in  $B$ -band,  $x_1$  is the stretch parameter,  $c$  is the color parameter,  $\alpha$  the stretch coefficient and  $\beta$  the color coefficient. The stretch and color parameters represent the sources of variability and are determined using spectral energy distribution models. The model we will use is the Spectral Adaptative Light-curve Template 2 (SALT2). The stretch parameter is an intrinsic parameter, it is related to the physical properties of the explosion. This parameter says that the luminosity of a SNe Ia at the maximum of luminosity increases with the time decay of the light curve. The color parameter can be intrinsic and extrinsic (presence of dust during the intergalactic journey). This parameter affects the luminosity of SNe Ia. The correlation of these two parameters to SNe Ia magnitude is shown in the **Fig.3**.

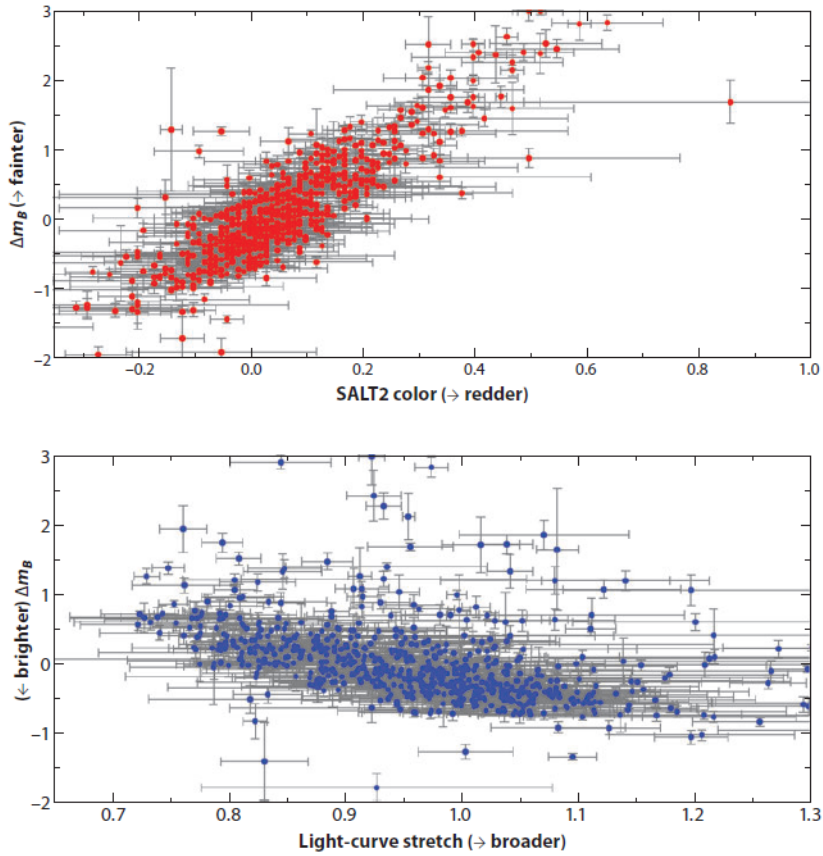


**Figure 3:** Stretch and color correlation with the magnitude from [8], Upper panel: the color correlation with the magnitude; Lower panel: the correlation between stretch and magnitude.

## C Hubble Tension

The Hubble constant  $H_0$  is the actual value of the expansion rate of the Universe, its measurement is therefore essential in cosmology. With what we have seen before there are two main methods for the measurement of  $H_0$  that stand out. The first one is to measure the distance of luminosity of SNe Ia and their redshift in order to build the Hubble diagram and to deduce the value of  $H_0$ . This measurement is purely geometrical and is based on a direct measurement because it makes the measurement at the current time, we speak more commonly of late measurement. The other method is an early method, because it is based on  $\Lambda$ CDM and the cosmic microwave background (CMB) radiation. This method consists then in adjusting the parameters of  $\Lambda$ CDM in order to find the CMB properties then to

retrace the history of the expansion of the Universe in order to arrive at the measurement of current  $H_0$ . These two measurements are independent of each other. We notice today that the more precise the methods are, the more they lead to two different and incompatible values of  $H_0$ . The latest direct measurements by the SH0ES<sup>5</sup> collaboration shows that  $H_0 = 73.04 \pm 1.04 \text{ km s}^{-1} \text{ Mpc}^{-1}$  while the indirect measurements by the Planck collaboration show that  $H_0 = 67.4 \pm 0.5 \text{ km s}^{-1} \text{ Mpc}^{-1}$ . We notice that these two values are totally incompatible and are  $5\sigma$  apart, we say that there is a  $5\sigma$  tension. We can see on **Fig.4** the illustration of this tension with different late and early measurements. Nowadays this tension is still not explained, is it a problem in the data for the direct measurement or that the model is incomplete for the indirect measurement. In this topic the study of potential anisotropies of  $H_0$  in the local Universe, by fitting the  $\Lambda$ CDM model with simulations of SNe Ia can bring new inputs in the debate.

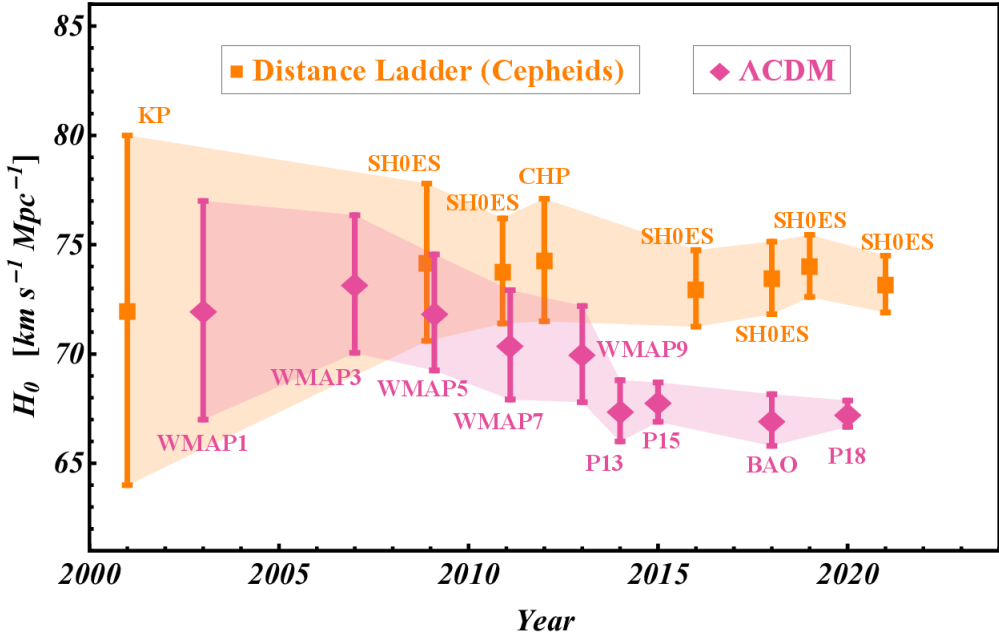


**Figure 4:** Hubble Tension, in orange direct measurement made with SNe Ia anchored on Cepheid and in pink indirect measurement with the  $\Lambda$ CDM model. This illustration comes from [10].

## II The Zwicky Transient Facility

The Zwicky Transient Facility (ZTF) is an astrophysical survey located at Mont Palomar in California. This survey allows us to observe the sky up to a limit of  $-30^\circ$  in declination ( $\delta$ ). The purpose of this part is to present the different components and the properties of ZTF in section A and the survey strategy in section B. This will allow a better understanding of how the simulations are made in part III. The part presented here is based on [11] and [4].

### A Architecture

For ZTF there are two phases of observation. The first, phase I, runs from 2018 to 2020 and the second, phase II, from 2020 to 2023. It is an experiment allowing to study for example Multi Messenger Astronomy, Solar system bodies etc. and of course to study the SNe Ia that it detects. ZTF has a large field of view of  $47 \text{ deg}^2$  which allows it to probe the northern sky with a high cadence.

ZTF uses the Polomar 48-inch Samuel Oschin Schmidt Telescope for its observations. This telescope alone does not allow the study of transient objects, the ZTF collaboration have made modernization modifications such as windshield refurbishment, better thermal management in the dome, electrical upgrades etc. They have especially improved the two drive axes of the telescope as well as

<sup>5</sup> Supernova H0 for the Equation of State

the dome drive system, these improvements allow the telescope to rotate and settle between adjacent fields entirely during the exposure and readout time of the Charge Coupled Devices (CCD). Indeed the most important improvement is that on the telescope is mounted with a new camera of CCD.

It is a camera of 600 mega pixels, consisting of 16 CCDs, these are large CCDs of  $6\text{k} \times 6\text{k}$ . If they are so large it is to fill the large surface of the telescope and to minimize the losses due to the spaces between the chips. Note that each CCD is divided into 4 read-out channels, these are the CCD quadrants (64 in all) and each quadrants corresponds to an image of about  $(0.8^\circ \times 0.8^\circ)$ . The exposure time is 30 seconds which allows ZTF to cover more than the accessible sky in one night.

Another important ZTF component is that it has three filters: ZTF-g (green), ZTF-r (red) and ZTF-i (infrared), these custom filters maximise the signal to noise ratio. The change of these filters is done through an ingenious mechanism with a robotic arm. For more technical detail on e.g. the cryostat or data acquisition please refer to [11].

## B Survey Strategy

As said before, ZTF is an international collaboration, so the observation time is divided into three main programs: public surveys (40%), ZTF collaboration surveys (40%) and Caltech surveys (20%). Of course in these programs sub-surveys share the allocated observation time. Note that the public surveys cannot use the ZTF-i filter, and their observations are public. The observation strategy of ZTF is based on two grids, each element of the grids is known as a field. The main grid uses 89% of the total observation time, as can be seen in **Fig.5**, which plots the main grid in the 3 bands as a function of the total number of exposures on the right panel, and as a function of the median delay between two consecutive exposures, that some areas are frequently observed. Taking into account that the exposure time is 30 sec, the observation rate is an important parameter of the survey. The second grid is a little bit shifted regarding the main one, and it is used for the calibration and also to avoid gaps between the CCDs, thus avoiding edge effects.

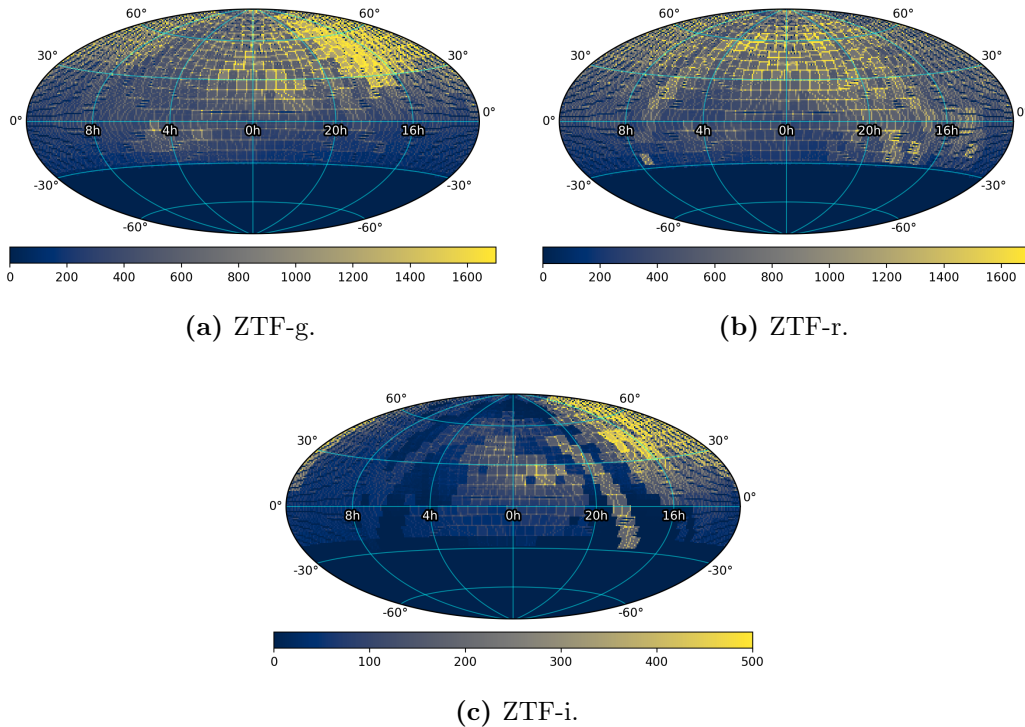


**Figure 5:** Sky coverage in equatorial coordinates (RA, DEC) and number of observation epochs for DR17 (up to 9 March 2023). (a): g-filter; (b): r-filter; (c): i-filter. Color bar represents the number of observation epochs. Dark regions on small scales are not holes in coverage, but due to the coarse resampling of CCD-quadrant centers on  $1^\circ$  scales. Figure that comes from [12].

## III Simulations

As our study is based on simulations, we will see in this part how these simulations have been produced in section A, then we will see in section B the selections we apply to obtain a realistic distribution of SNe Ia.

### A simssurvey

For simulations we use `simsurvey`. Making a simulation of a survey is dependent on several factors that must be taken into account as the cadence, the choice of filter, sky coverage etc. `simsurvey` is a Python code that is made in such a way that we can change details of the survey to suit the survey and the transient models. This code uses the `sncosmo` and `astropy` packages. `simsurvey` is used to simulate light curves of several SNe types. Several inputs are then required: the time, pointing and filter of each exposure and for each observation the sky brightness and zero point (ZP, see equation III.1 for its definition); we also need to choose a transient model i.e. time-series of spectral energy distributions. And finally we need a function allowing the sample transient model parameters like for example peak magnitude. The transient objects are placed at sampled redshifts. The total number of transients generated depends on the integrated rate, the duration of the survey and the solid angle it covers. `simsurvey` then outputs for each transient coordinates on the sky thanks to a uniform distribution on the unit sphere, the extinction of the Milky Way is taken into account thanks to galactic dust maps so that the light curves of the transients behind this dust will be below the threshold of detection. The code also outputs a random Julian date for the parameter  $t_0$  (peak magnitude in *B*-band of the light curve) by a uniform distribution, this date is included in the duration of the chosen study. For the other parameters of the light curves simulations, they are determined with the redshifts and the transient model. In the model parameters there are generally the normalization of the model flow and the specific parameters of the model (e.g.  $x_1$  and  $c$  the parameters of SALT2). With these parameters `simsurvey` simulates the light curves based on the survey schedule. The list of observations is restrained by the minimum and maximum time relative to  $t_0$  which allows to limit the light curves to the relevant parts. The time frame is extended by two weeks before the model definition range which allows to evaluate if there are pre-explosion limits for the transient. The light curves are then filtered with selection criteria corresponding to the discovery process of the transient records. Note that there needs to be two  $5\sigma$  detections in the same night for a transient to be included in the final output. For more details on `simsurvey` please refer to [13].

We can then run the simulations for ZTF. In our subject we use Melissa ZTF-log, a code developed by Melissa Amenouche, which is a code that tuned `simsurvey` to do the simulation of SNe Ia as obtained by the SNe Ia Data Release 2 (DR2). DR2 represents the first 3 years of ZTF observation.

### B Supernova selection

Once the simulations are done we need to make different selections to determine if the simulated supernovae are realistic. To understand the transient effects we need to know the classification and redshift of each object. So we use spectroscopy, this is what the Bright Transient Survey (BTS-[14] and [15]) working group does, they classify the brightest transient discovered by ZTF. The spectroscopic selection of BTS is done by selecting the brightness peaks of the transient and their light curves. We therefore use the spectroscopic selection function of BTS which we fit by a sigmoid function as in Fig.6a. We need to calculate the maximum magnitude of each SNe Ia simulated and then thanks to this and the sigmoid function that depends on the magnitude we determine the associated classification efficiency. The magnitude is calculated from the maximum of the flux of the simulated light curves as follows:

$$m = -2.5 \log_{10}(\max(f_{ADU})) + ZP \quad (\text{III.1})$$

where  $f_{ADU}$  is the flux in Analog to Digital Unit (ADU) which is a quantity proportional to the number of incident photon and ZP is the zero point associated with the max of the flux which is the calibration coefficient to translate the measures flux in a magnitude system. Then a number is

### III SIMULATIONS

randomly and uniformly drawn between 0 and 1. If the value drawn is less than the classification efficiency then the SNe is not selected, otherwise it is selected. We can see on **Fig.6b** the comparison of distribution before and after the spectroscopic selection.

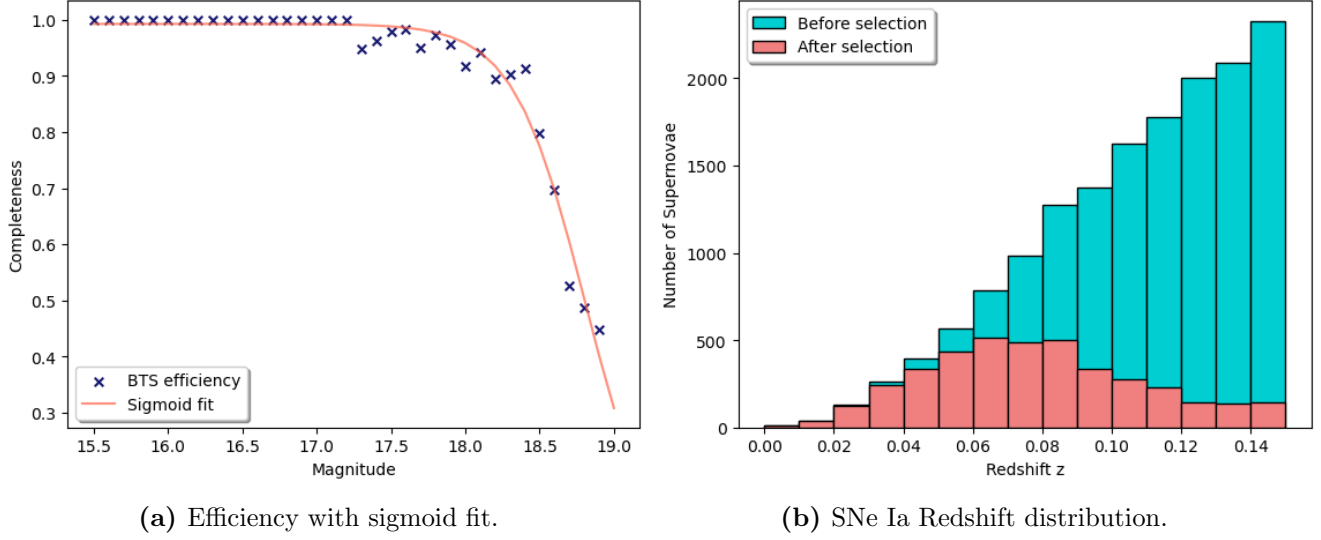


**Figure 6:** BTS spectroscopic selection: (a) Line represents the sigmoid fit and point are obtained from BTS, (b) Redshift distribution of simulated SNe Ia that passed the spectroscopic selection.

We must then take into account the galactic extinction. We first do as in BTS analysis, a cut on the coordinates, we remove all the supernovae that have a galactic latitude (b):  $-7^\circ < b < 7^\circ$ . In addition we make a selection on the fact that the Galactic extinction should be low ( $A_V < 1$  mag).

The simulated SNe must then pass further selections. These selections are multiple and are summarized in table 1. There are selections on the light curves, on their number of points and their relative uncertainties to eliminate the bad light curves as in **Fig.7b**. In table 1 there are also selections on the cosmological parameters as in BTS.

Parameter	criteria	interval	relative uncertainty
$N_{point}$	$\geq 7$	$[t_0 - 15 \text{ days}; t_0 + 30 \text{ days}]$	$\geq 5$
g and r filter	1 point	before and after $t_0$	$\geq 5$
$ x_1 $	$\leq 4$		
$c$	$\in [-0.3; 0.8]$		
$\sigma_{x_1}$	$< 1$		

**Table 1:** Criteria selections.

### III SIMULATIONS

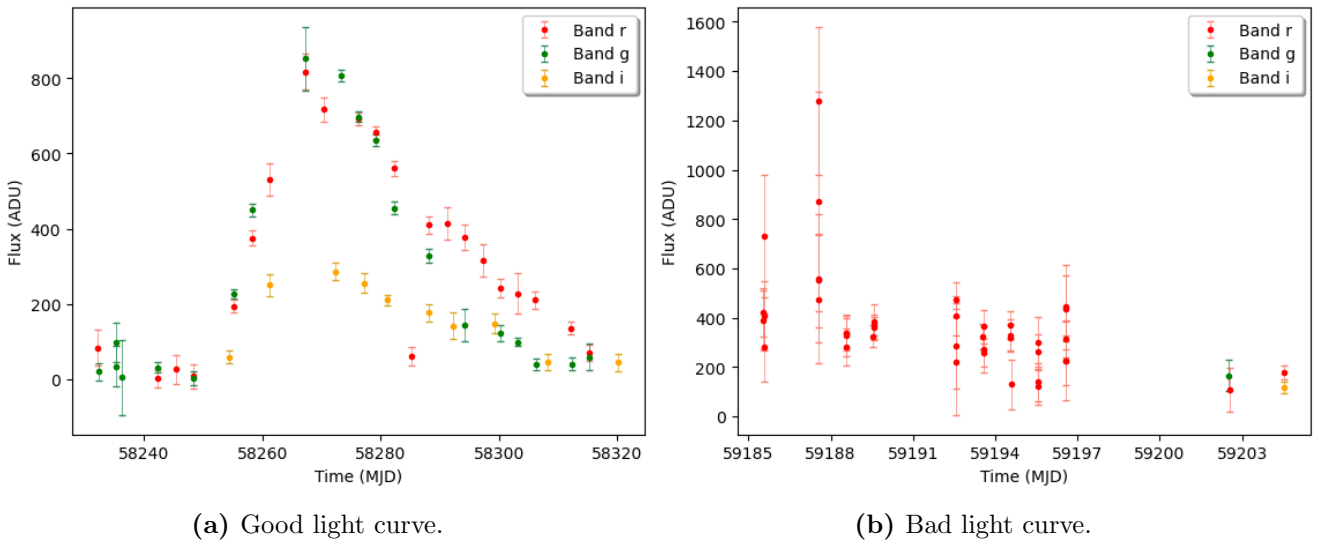


**Figure 7:** Light curves: (a) A light curve that we can take into account because it is well defined, (b) A bad light curve because there is a lack of point in g-band and large errors on the points.

After all these selections we get about 2500 SNe Ia over three years of survey. **Fig.8** shows the distribution of the selected SNe Ia in equatorial coordinates. We notice that the distribution in redshift seems uniform as expected and we notice the delimitation with the Milky Way.

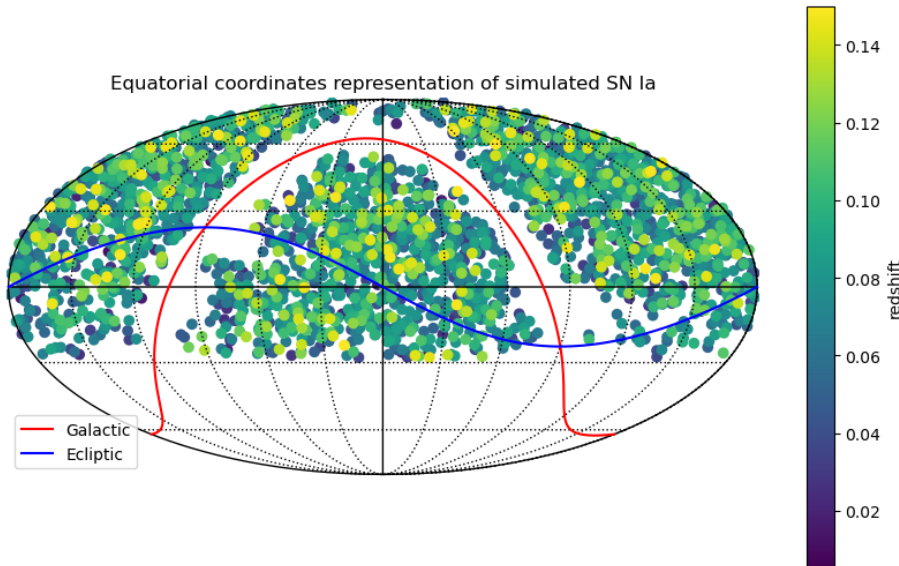


**Figure 8:** Sky map of SNe Ia selected according to their redshift (color): red line is the galactic plane and the blue line is the ecliptic plane, the distribution seems to be uniform.

## IV Anisotropies Analysis

With all the tools we have just seen we can now make the analysis of possible anisotropy in the Hubble constant. We will start from an analysis on the set of SNe Ia in order to build the associated Hubble diagram. Then we will see the partitioning methods used and finally we will do the analysis on the variations of  $H_0$ .

### A Hubble Diagram

Using equation I.23 we can construct the Hubble diagram for the simulated SNe Ia, i.e. the distance modulus as a function of the redshift. This diagram is represented on **Fig.9a**. On this figure it is also represented the distance modulus but without the standardization, we notice then that the terms of color and stretch avoid a dispersion of the points. Note that the values of  $m_B^*$ ,  $x_1$  and  $c$  are given by the fit of light curves thanks to SALT2 while  $M_B$ ,  $\alpha$  and  $\beta$  have been fixed with values close to what we find in the literature. Now that we have these distance modulus, we need to leave  $M_B$ ,  $\alpha$  and  $\beta$  free and be able to find them by fitting the points with the distance modulus of the  $\Lambda$ CDM (equation I.22). At first we leave  $\Omega_m$  free to see what changes, but finally we realize that  $\Omega_m$  does not make a low redshift lever arm like here so we fix it to a typical value of cosmological analysis  $\Omega_m = 0.3$ . So we build the  $\chi^2$  as follow:

$$\chi^2 = \sum_i^{N_{SNe}} \left( \frac{\mu_i - \mu_{\Lambda CDM}(z_i)}{\sigma_i} \right)^2 \quad (\text{IV.1})$$

where  $\sigma_i$  is the uncertainty on the distance modulus of the simulated SNe Ia, defined as:

$$\sigma_i^2 = \sum_{k,l} \left( \frac{\partial \mu_i}{\partial x_k} \right) \left( \frac{\partial \mu_i}{\partial x_l} \right) V_{k,l} + \sigma_{\Lambda CDM}^2(z_i) \quad (\text{IV.2})$$

where  $V_{k,l}$  is the covariance matrix of SALT2 light curve fit and  $k,l = m_B^*, x_1, c$ .  $\sigma_{\Lambda CDM}(z_i)$  is the uncertainty for the  $\Lambda$ CDM distance modulus, expressed as:

$$\sigma_{\Lambda CDM} = \left| \frac{\partial \mu}{\partial z} \right| \sigma_z \quad (\text{IV.3a})$$

$$= \frac{5}{\ln 10} \left[ \frac{1}{1+z} + \frac{1}{\chi \cdot H(z)} \right] \sigma_z \quad (\text{IV.3b})$$

where

$$\chi = \int_0^z \frac{dz'}{H(z')} \quad (\text{IV.4})$$

with  $\sigma_z = 0.5 \times 10^{-3}$  the typical uncertainty on the redshift determination of the host galaxy of SNe Ia. The  $\chi^2$  allows to check if the observed value corresponds to the expected one. The lower the  $\chi^2$ , the more the values obtained correspond to the model. To make the fit of the Hubble diagram we make the minimization of  $\chi^2$  thanks to `iminuit` using the package `Minuit`. This package allows to make the Least Squares minimization and to return the fitted parameter corresponding to this minimization made with `migrad()`. `migrad()` uses the approximate first and second derivatives to reach a quadratic convergence close to the minimum<sup>6</sup>. By doing the  $\chi^2$  minimization, `Minuit` returns the fitted parameters of **Table 2**. In this fit the Hubble constant is fixed to an average value of  $H_0 = 70 \text{ km s}^{-1} \text{ Mpc}^{-1}$  because it is degenerated with  $M_B$ .

Parameter	Value	Uncertainty
$M_B$	-19.0958	0.0019
$\alpha$	0.1227	0.0018
$\beta$	2.970	0.018

**Table 2:** Global fit values

<sup>6</sup> <https://iminuit.readthedocs.io/en/stable/>

The values are obtained with small errors. We can then represent the new Hubble diagram with the fitted parameters as shown in the **Fig.9b**. In **Fig.9b** it is represented the residues to see to which point we depart from the model or not. We notice that the  $\chi^2$  per degree of freedom is close to 1 so our values are not so far from the model. Note that the error bars are given by the equation IV.2. We notice that we obtain a standard deviation of about 0.11 for the residuals ( $\mu - \mu_{\Lambda CDM}$ ) which is a typical value in Hubble diagram. Note that the result of this global fit will be used for the rest of the analysis.

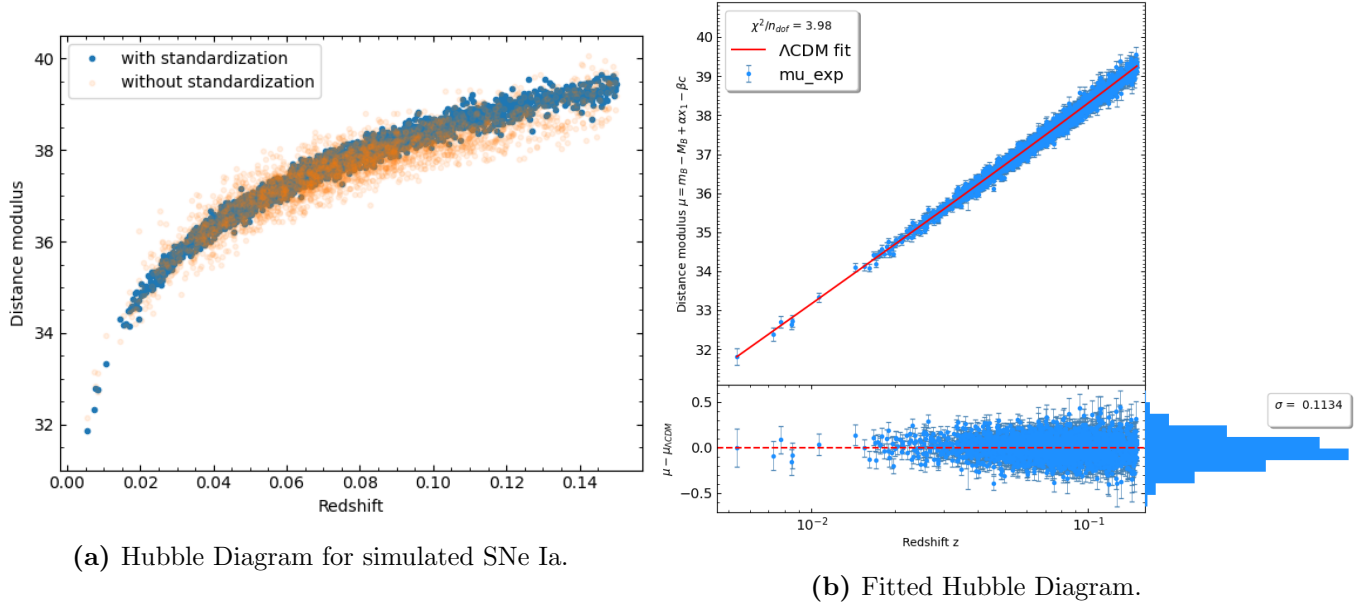


**Figure 9:** Hubble Diagram: (a) In blue the points with the stretch and color parameters correction. In orange without standardization, (b) The Hubble diagram: the red line represents the  $\Lambda$ CDM model and the points are the distance modulus of the SNe Ia.

## B Partitionning

To make an analysis of potential anisotropy it is necessary to determine directions and area of the sky to observe and compare. For this we have chosen two methods. The first is to use HEALPix to define patches of unmovable sky, while the second is based on the distribution of SNe Ia through a clustering algorithm.

### B.1 HEALPix

In order to partition the sky map and represent each selected sky direction by their possible anisotropies we use `healpy`<sup>7</sup>, the python software version of HEALPix (Hierarchical Equal Areas isoLatitude Pixelisation). It is thus an algorithm of pixelization of a sphere. We need to understand how the sphere is pixelated to be able to partition the map. The `healpy` package allows many things like a representation in different projections, allows pixelization, contains several routines, spherical harmonic etc. For our subject we will use mainly pixelization and graphic projections. We define the number of divisions along the side of a basic resolution pixel with  $N_{side}$ . All pixels have a center associated with spherical coordinates, each center is placed on  $4 \times N_{side} - 1$  rings of constants latitude and are equidistant in azimuth. The total number of pixels is given by  $N_{pix} = 12 \times N_{side}^2$ . We notice on **Fig.10** which represents different resolutions that the pixels of lower resolution are subdivided to reach the other resolutions.

<sup>7</sup> <https://healpy.readthedocs.io/en/latest/>

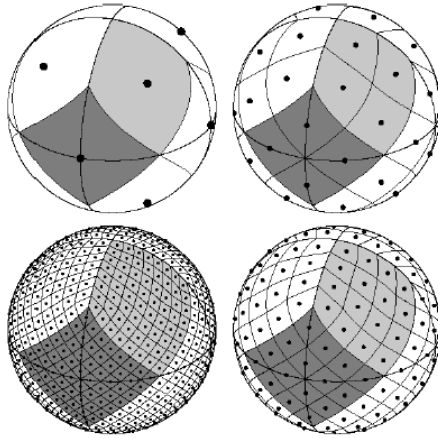


**Figure 10:** Orthographic view of HEALPix partition of the sphere: for  $N_{side} = 1, 2, 4, 8$  (from top-left in clockwise; the figure comes from [16].

A last point that interests us is that each pixel has an index. There are two ordering methods in HEALPix. The first one consists in numbering the pixels from 0 to  $N_{pix} - 1$  starting from the north pole to the south pole considering the circles, it is the Ring ordering. The second method is the Nested ordering. In this method the indexing is based on the pixels of lower resolution. Example pixel indexed 0 of lower resolution ( $N_{side} = 1$ ) is subdivided in four pixels numbered from 0 to 3 ( $N_{side} = 2$ ), then pixel indexed 1 of lower resolution is subdivided into 4 to 7 indices etc. Note that `healpy` contains a method for converting indices between the two methods.

We can make the same representation as in **Fig.8** but with the pixelization. The difference here is that we assign the SNe Ia to pixels according to their coordinates and we illuminate the pixel with the associated redshift value.

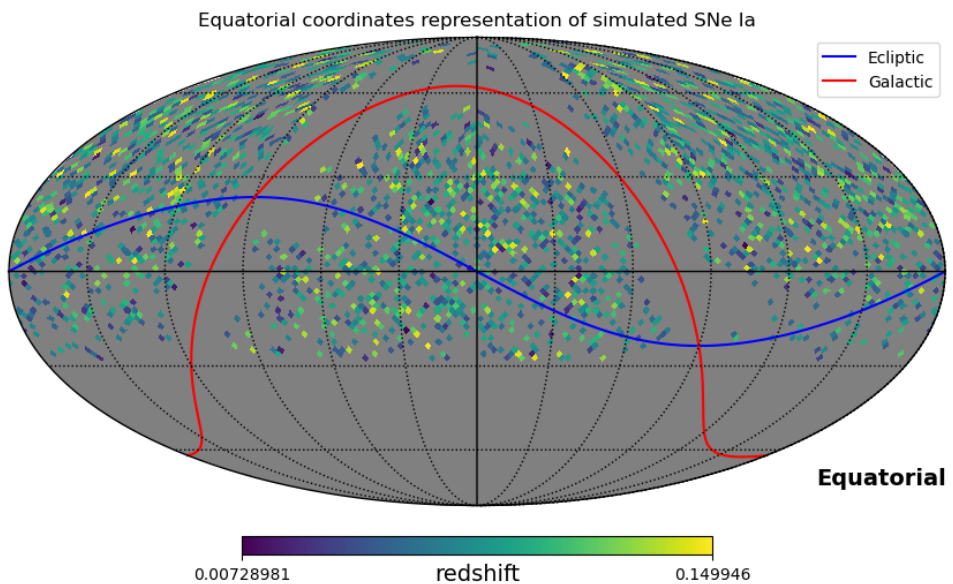


**Figure 11:** Pixel representation of the SNe Ia distribution on equatorial coordinate: red line is the galactic plane and the blue line is the ecliptic plane.

The disadvantage of this representation is that if the resolution is too low there may be several SNe Ia in the same pixel and if we increase the resolution the representation becomes unreadable because the pixels becomes too small. However, in the method used we can make this pixelation very high but we will not represent it with the distribution.

## B.2 HEALPix Method

The method that uses HEALPix is to use a low resolution, for example here we will use  $N_{pix} = 12$ , it is then enough to use the method `ang2pix` of `healpy` which allows to change the coordinates of points in indices of pixel according to the resolution chosen. We decide to do this for each SNe Ia, then their pixel indices correspond to the patch to which they belong. We can see on **Fig.12** the distributions of supernovae in redshift and also the number of SNe Ia in each patch.

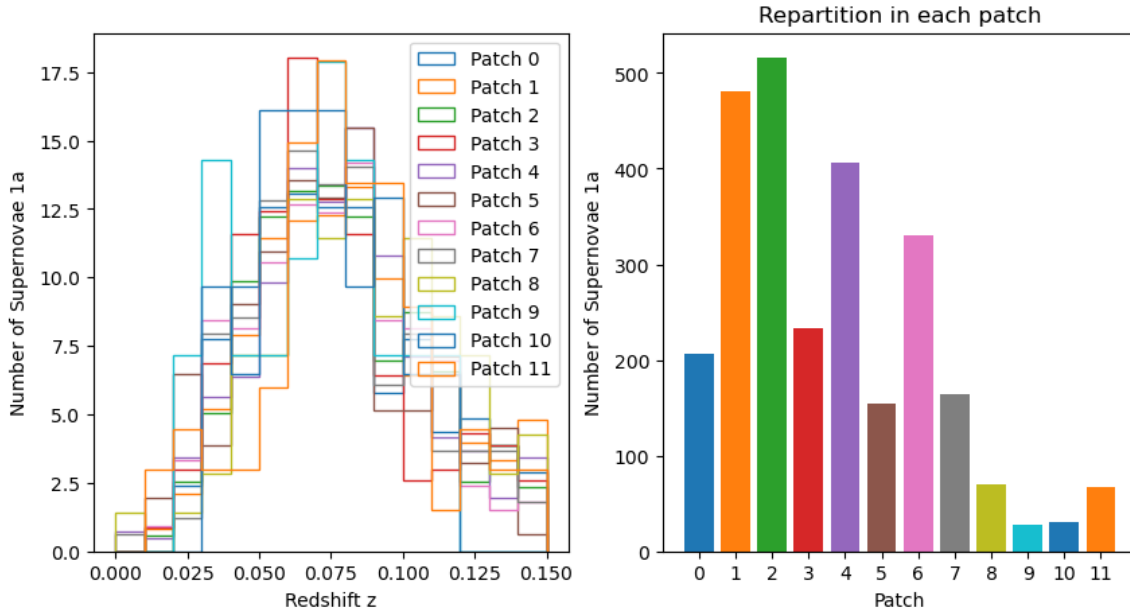


**Figure 12:** Distribution per patch: left panel represents the normalized redshift distribution per patch, right panel represents the number of SNe Ia per patch.

We notice that some patches have very little SNe, we will see later if this has an impact on the analysis. Note that the redshift distributions per patch seem similar to the global distribution for patches that contain enough statistics. For the following we will represent each patch with their value of variation of  $H_0$ , however it should not be displayed for  $\delta < -30^\circ$  and in the galactic plane. The method to do this is to use a strong resolution and the `nest2ring` method which changes the pixel indices from Nested ordering to Ring ordering. With this way we can more easily find the pixel indices to be shaded.

## B.3 Clustering Algorithm

The second method chosen to partition the sky map is to use a clustering algorithm on the coordinates of the SNe Ia and to group them by cluster. We use the Kmeans algorithm thanks to `sklearn.cluster.Kmeans`. The algorithm is simple, we randomly select K initial centers, we then assign each data to the nearest centroid, if the partition doesn't change the process is stopped, else update centers i.e. centers are recalculate with each data that correspond with a center and remake the process. To choose the ideal K number of cluster we use the Elbow method, this method consists in plotting the sum of squared error in function of number of cluster and choose the elbow of the curve as number of cluster to choose. The **Fig.13** represents the Elbow method. Graphically we choose to make 11 clusters.

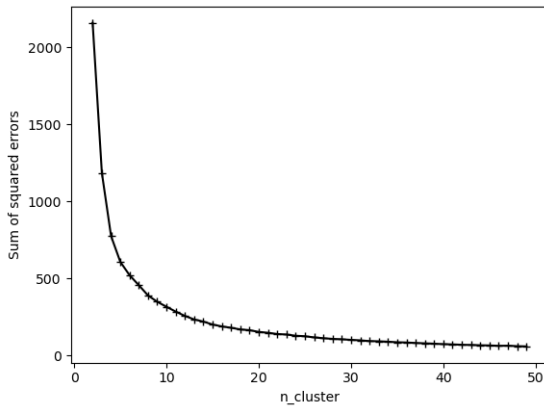


**Figure 13:** Elbow method: sum of squared error in function of number of cluster

The **Fig.14** represents the distribution in each patch. We notice that with this method the number

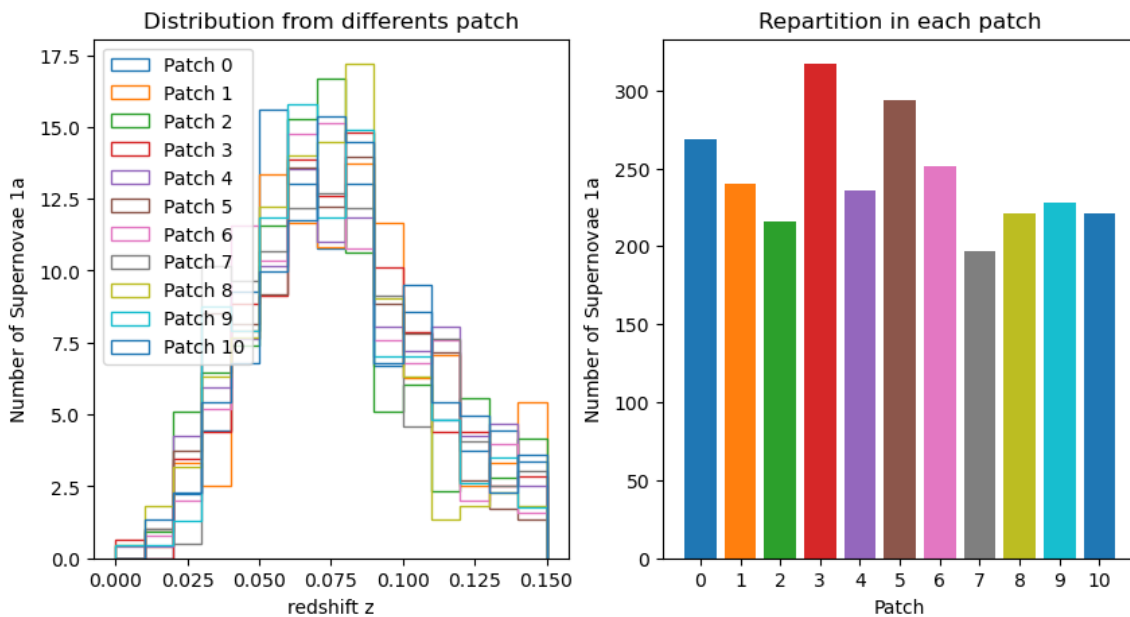


**Figure 14:** Distribution per patch: left panel represents the normalized redshift distribution per patch, right panel represents the number of SNe Ia per patch.

of SNe Ia per cluster seems to be well balanced, we also notice about the same distribution in redshift. However the disadvantage of this method is that the definition of the patches depends on the initial parameters for clustering. To make the visual representation of the patches it is enough to recover the previous final centroids and to redo an algorithm of Kmeans by entering these centroids in initial parameter and to make only one iteration but on the pixels. Indeed each pixel is attached to a coordinate, it is then enough after removing the pixels where we have no data and we get the desired representation. Other methods have been tried like the direct clustering on the pixels or by using the `query_polygon` routine (see [Appendix 1](#)). We didn't choose them because they were either too hard to set up and not very optimized or lacked of precision.

## C $H_0$ Variations

Now, we have all the tools to make an anisotropy analysis we will see in this part the method to enter a variation of  $H_0$  then we will make the fit for the partitioning methods seen before and finally we will compare them.

### C.1 Method

We seek to fit the variation of  $H_0$  according to the patch, we must then add a variation  $\delta H_0$  to the expression of the distance of luminosity (equation I.20). The equation IV.1 expressing the  $\chi^2$  becomes:

$$\chi^2 = \sum_j^{N_{cluster}} \sum_{i_j}^{N_{SN}} \left( \frac{\mu_{ij} - \mu_{\Lambda CDM}(z_{ij}, \delta H_0)}{\sigma_{ij}} \right)^2 \quad (\text{IV.5})$$

where  $\delta H_0^j$  is the variation of  $H_0$  in cluster number  $j$  with respect to the baseline value  $H_0 = 70 \text{ km s}^{-1} \text{ Mpc}^{-1}$ . To be able to do the minimization of this  $\chi^2$  and to find the  $\delta H_0$  fit we have to fix  $M_B$  with the value obtained by the global fit because  $M_B$  and  $H_0$  are degenerate (see Appendix 2 for the demonstration). Note that we leave free  $\alpha$  and  $\beta$  which are common to all patches i.e. we assume that all SNe Ia are standardized in the same way, what ever is the direction in the sky.

### C.2 Analysis with HEALPix Patch

The partitioning method with HEALPix gives the values obtained in Table 3 in the Appendix 3 for 12 patches. We represent these values of  $\delta H_0$  on Fig.15a. The Fig.15b represents on the top panel the value of the Hubble constant for each patch with the associated uncertainties obtained by the minimization while the bottom panel represents the average value of the residual per patch.

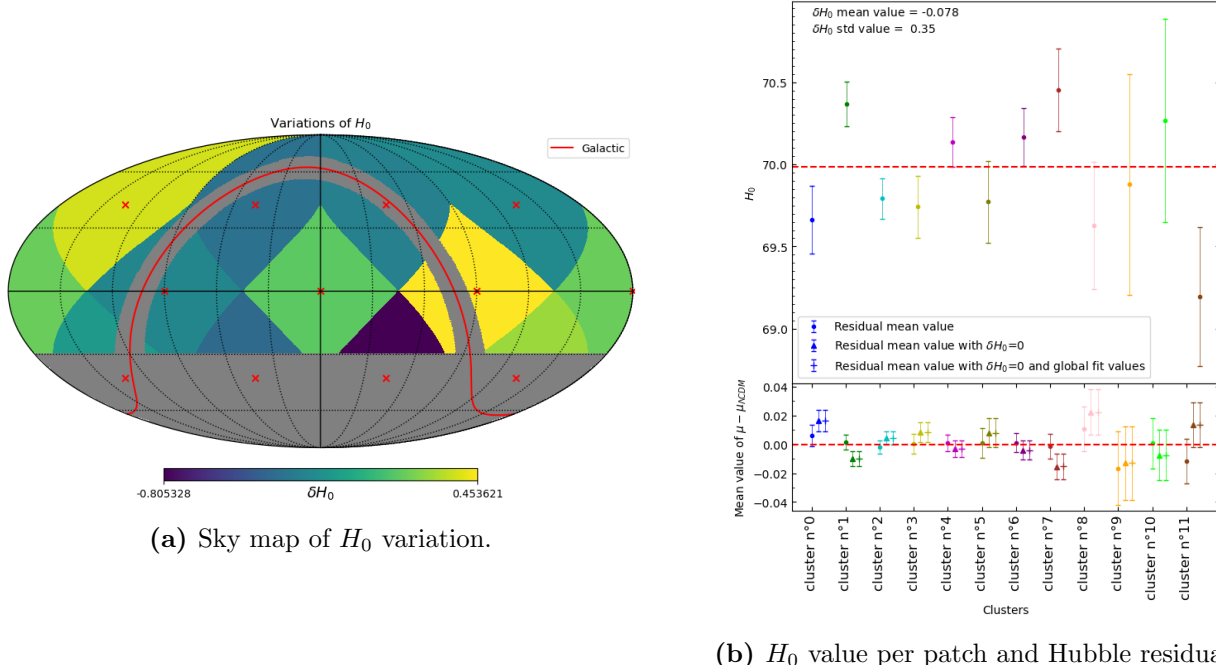


**Figure 15:**  $H_0$  variations for HEALPix method: (a) red line represents the galactic plane and color represents  $\delta H_0$  value , (b) top panel:  $H_0$  value per patch with red dotted line the mean of  $H_0$ ; bottom panel: points residual mean value, triangle the mean value with  $\delta H_0 = 0$ , cross the mean value with  $\delta H_0 = 0$  and global fit parameter values.

The error bars are:

$$\sigma^j = \frac{\sigma_{res}^j}{\sqrt{N_{SN}^j}} \quad (\text{IV.6})$$

We notice that the last four patches have very large errors which corresponds to the southern most patch where the statistics are low. On the bottom panel of Fig.15b we notice that the parameters  $\alpha$  and  $\beta$  common to each patch correspond with the global fit values. Fig.16 illustrates the Hubble diagram for a patch with a high statistic and one with a low statistic.

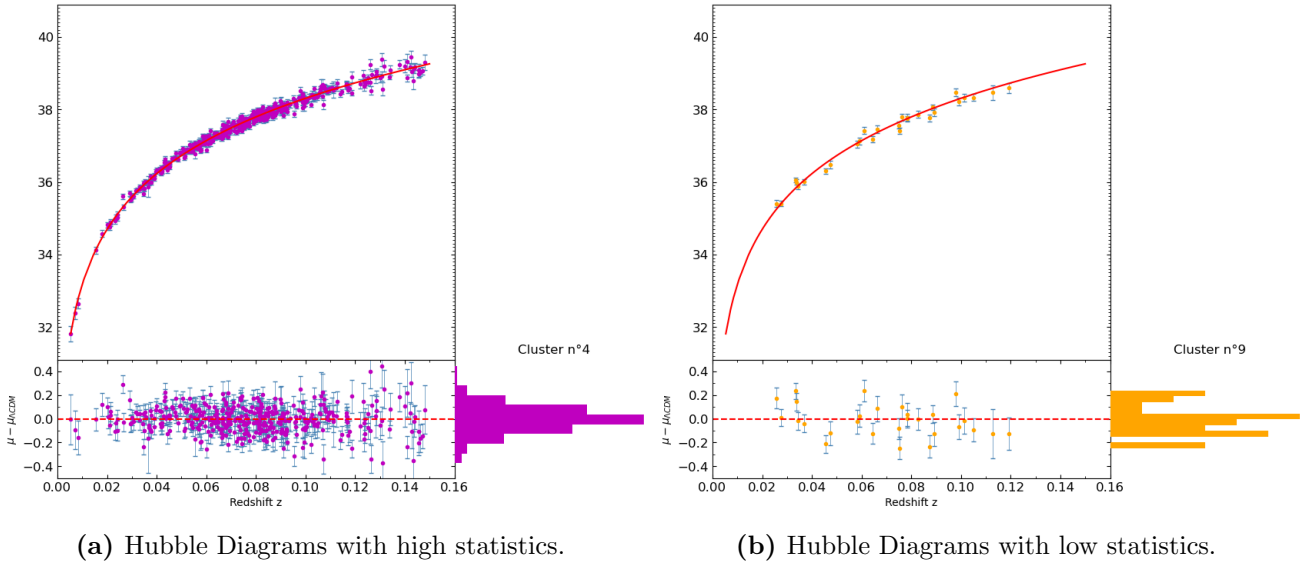


**Figure 16:** Hubble Diagrams for specific patch: (a) excellent distribution and many statistics , (b) low distribution and less statistics.

We notice on **Fig.16** the difference in statistics, the distribution is not uniform for a patch that lacks statistics. The lack of statistics in some few patches is therefore a huge inconvenience because it introduces significant errors, we must look for a method that allows us to make patches with equivalent statistics like with the clustering method.

### C.3 Analysis with Clustering Patch

We repeat the previous analysis for the clustering method. We obtain for 11 patches the values in **Table 4** in the [Appendix 3](#). We see on **Fig.17a** the sky map of  $H_0$  variations and on **Fig.17b** the values of  $H_0$  obtained as well as the average value of residual per patch. We notice that contrary to the previous method, all patches have comparable errors and we are close to the  $\Lambda$ CDM.

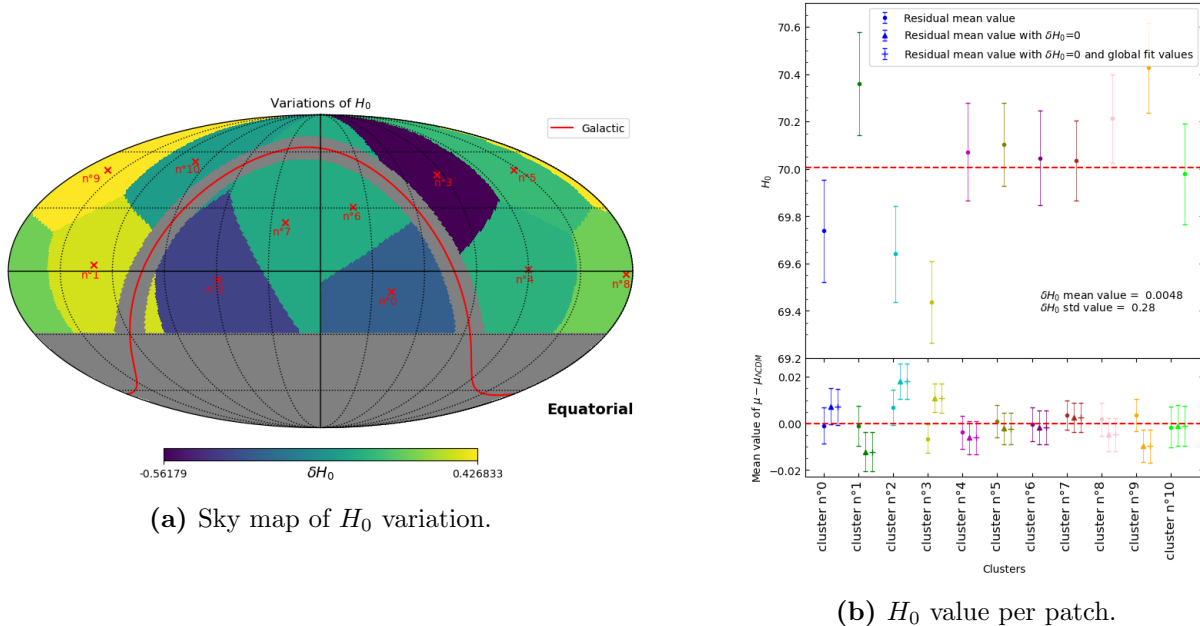


**Figure 17:**  $H_0$  variations for clustering method: (a) red line represents the galactic plane and color represents  $\delta H_0$  value , (b) top panel:  $H_0$  value per patch with red dotted line the mean of  $H_0$ ; bottom panel: points residual mean value, triangle the mean value with  $\delta H_0 = 0$ , cross the mean value with  $\delta H_0 = 0$  and global fit parameter values.

#### C.4 Comparison

In this first analysis, no anisotropy is introduced, so it allows to quantify the sensitivity of ZTF to measure deviations. We have therefore realized ten simulations, we can see on **Fig.18** the comparison on mean value and standard deviation of  $\delta H_0$  between the two methods on several simulations. We notice for the average value of  $\delta H_0$  that there is less dispersion for the clustering method as well as for the standard variation, moreover the variation is a little bit lower for the clustering method.

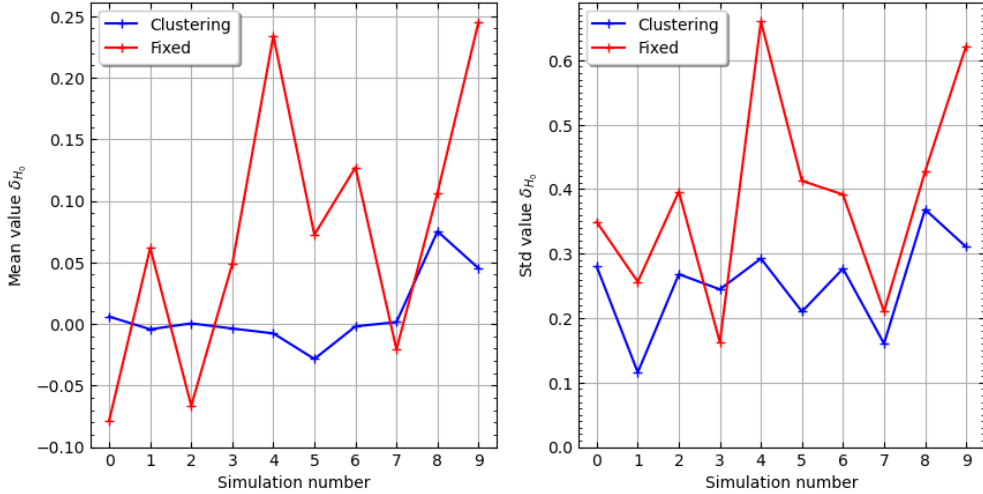


**Figure 18:** Comparison between HEALPix and clustering method. Left panel: mean value, right panel:  $\delta H_0$  standard deviation.

As suggested in [3], we will now introduce a tilt with a dipole shape. The goal is to see if we can find with the fit an anisotropy that we would have introduced in the simulations.

## D Dipole Introduction

We have seen previously an analysis without  $H_0$  anisotropy. So the goal of this part is first to introduce a dipole anisotropy effect in the simulations and then to do the analysis with the minimization and see if we find the dipole.

### D.1 Dipole Effect

We seek to place ourselves in a dipolar cosmology as in [3] to reveal anisotropy along a tilt. Therefore, we add a dipole effect on the variations of  $H_0$  in the redshift of the simulations. To do this we start from Hubble's law (equation I.15) which we modify as follows:

$$cz' = H'_0 d \quad (\text{IV.7a})$$

$$= (H_0 + \delta H_0(\Delta\theta))d \quad (\text{IV.7b})$$

$$= H_0 \left( 1 + \frac{\delta H_0}{H_0} \cos(\Delta\theta) \right) \frac{cz}{H_0} \quad (\text{IV.7c})$$

Finally:

$$z' = \left( 1 + \frac{\delta H_0}{H_0} \cos(\Delta\theta) \right) z \quad (\text{IV.8})$$

where  $\Delta\theta$  is the angle between the dipole and a supernova. As in [3] the redshift is chosen to be along the cosmic flux, i.e. along the tilt of the dipole. The map of anisotropy is represented in **Fig.19** for  $\delta H_0 = 5 \text{ km s}^{-1} \text{ Mpc}^{-1}$ .

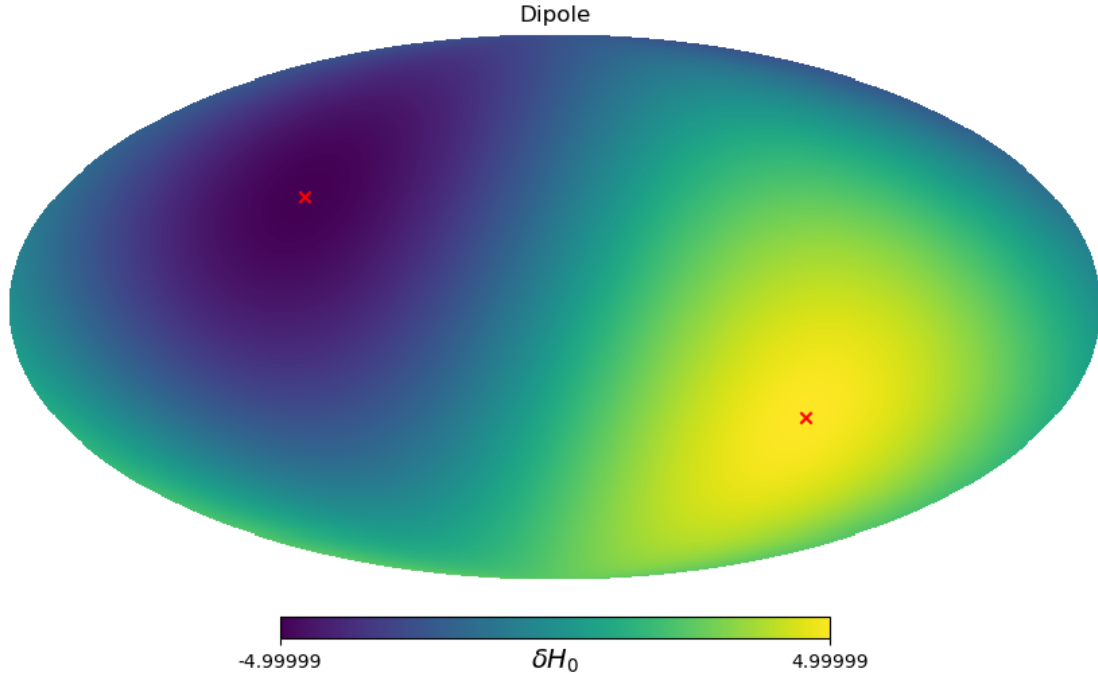
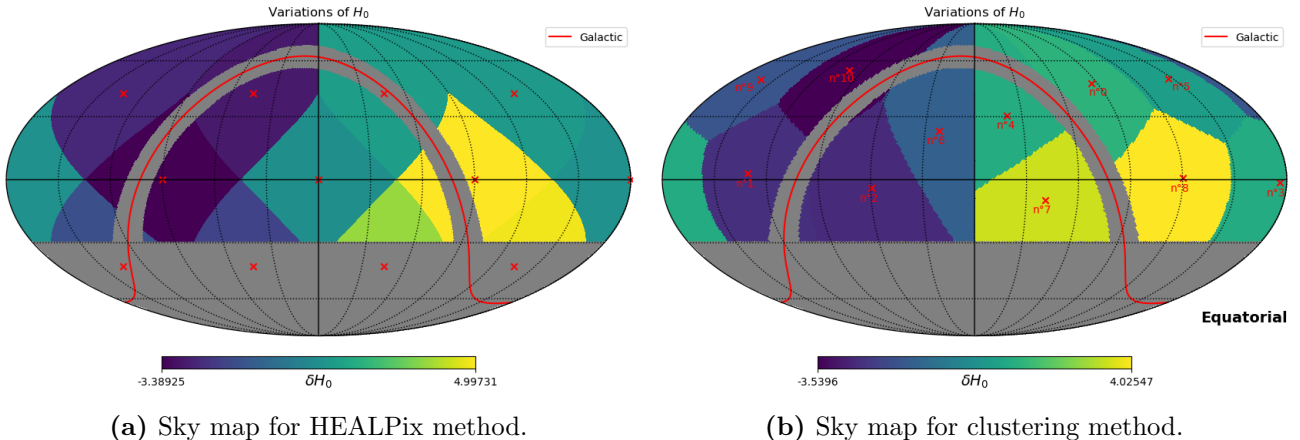


**Figure 19:** Dipole anisotropy effect Map: colors correspond to the  $\delta H_0$  value and crosses are dipole direction.

We have therefore generated our tilt, we can very clearly distinguish the two poles with the variation of  $5 \text{ km s}^{-1} \text{ Mpc}^{-1}$ . It is then necessary to do the fit to see if we find these variations on the tilt.

## D.2 Analysis with the two Partitioning Methods

We realize the fit for both partitioning methods. We obtain the map shown in **Fig.20**.



(a) Sky map for HEALPix method.

(b) Sky map for clustering method.

**Figure 20:** Sky map for dipole: (a) HEALPix method , (b) clustering method.

We note that we find the same aspect as in **Fig.19**. However, we do not obtain exactly the right interval of  $\delta H_0$  due to the low resolution because the point where  $\delta H_0 = 5 \text{ km s}^{-1} \text{ Mpc}^{-1}$  is exactly on the pixel of the dipole. On this figure we notice that the method of fixed patches seems to be closer to the variation put in input. However, to verify this, it must be done on several simulations. Another test that could be done is to increase the granulometry of the patches to see if we get closer to the input variation. We can also represent the values per patch on **Fig.21**.

We notice in **Fig.21**, which represents the values of  $H_0$  with the associated variations as well as the residuals of the distance modulus, that the values of the Hubble constant deviate quite significantly from the input value. The standard deviation on the  $H_0$  variations are around  $2.5 \text{ km s}^{-1} \text{ Mpc}^{-1}$ .

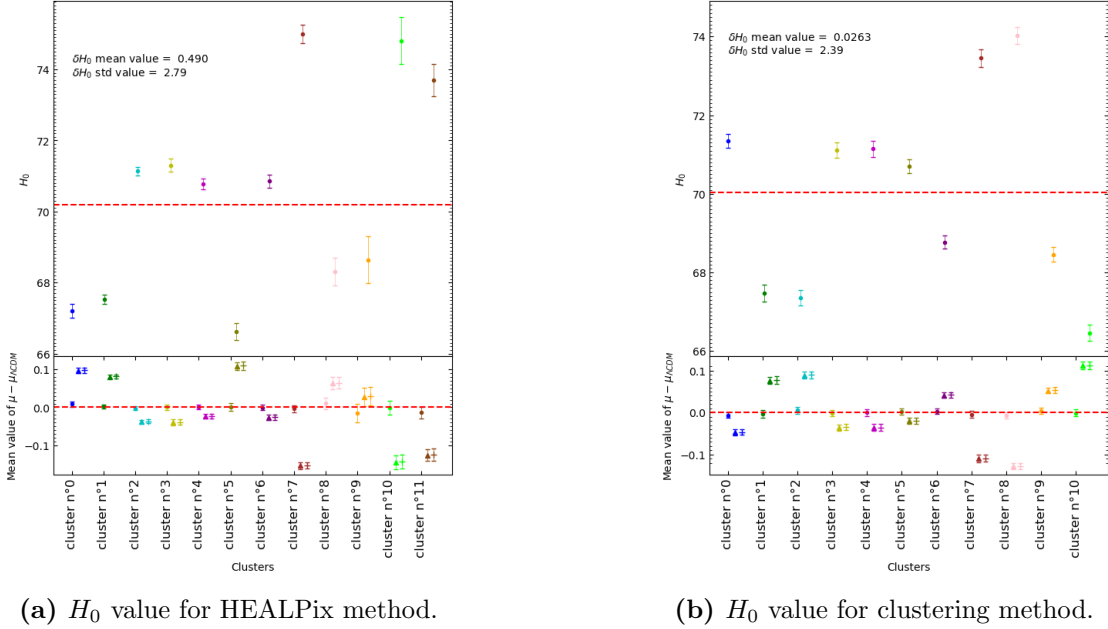


**Figure 21:**  $H_0$  value for dipole effect: (a) HEALPix method , (b) clustering method.

Now we would have to see if starting from the  $H_0$  variations obtained we could not find the amplitude and the direction of the introduced dipole, i.e. make a reverse fit.

### D.3 Reverse Fit

To find the amplitude and the direction of the introduced dipole, we need to recover the values of  $H_0$  obtained in the previous analysis as well as the associated uncertainties. Moreover, the theoretical  $H_0$  is constructed as:

$$H'_0(\Delta\theta) = H_0^{input} + \delta H_0^{input} \cos(\Delta\theta) \quad (\text{IV.9})$$

where  $\Delta\theta$  depend on dipole equatorial coordinates. Therefore the  $\chi^2$  is constructed as follow:

$$\chi^2 = \sum_i^{N_{cluster}} \left( \frac{H_0^i - H'_0(\Delta\theta_i)}{\sigma_{H_0^i}} \right)^2 \quad (\text{IV.10})$$

The results obtained by minimizing the  $\chi^2$  with the same previous simulations are shown in **Fig.22**.

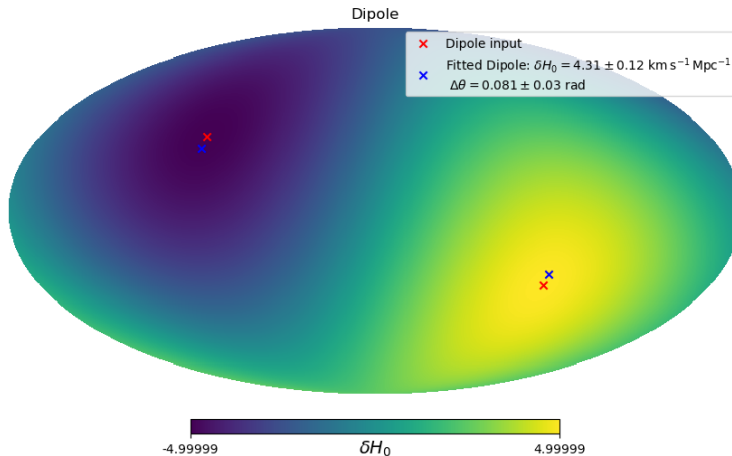


**Figure 22:** Dipole anisotropy map with fitted directions: colors correspond to the  $\delta H_0$  value, red crosses are input dipole direction and blue crosses are fitted dipole direction with an amplitude of  $4.31 \text{ km s}^{-1} \text{ Mpc}^{-1}$ .

We note that we are close to the input values in both amplitude and direction. This analysis needs to be verified on the other nine simulations, and with different input amplitudes and directions. **Fig.23** shows the distribution of deviations between the values obtained by the fit and the input values.

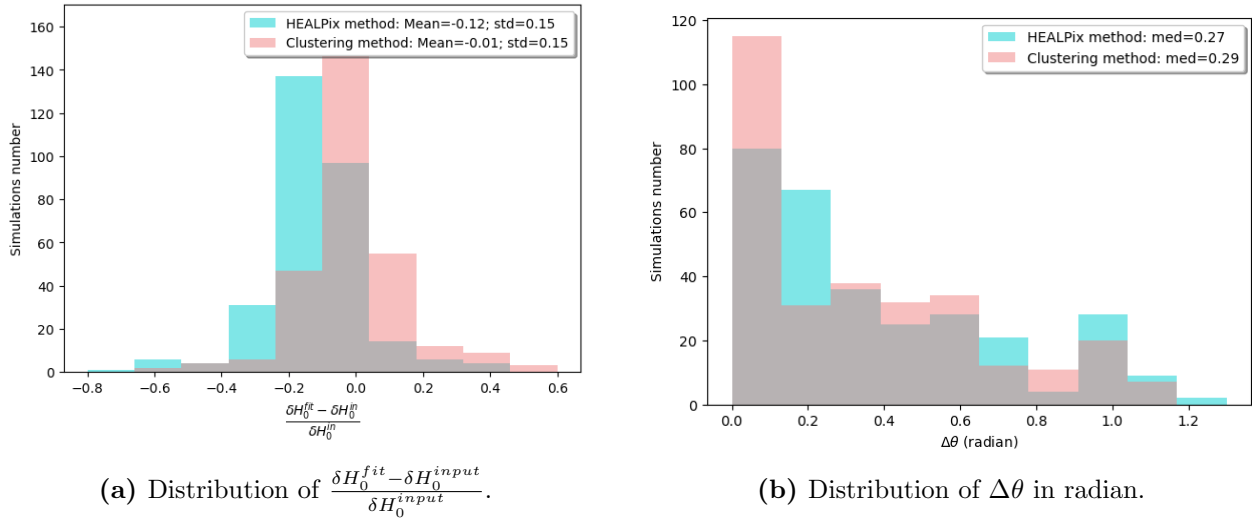


**Figure 23:** Distributions of the difference between fitted dipole and input dipole: (a) the distribution for the  $H_0$  variations , (b) distribution for  $\Delta\theta$  which represents the angle between input dipole and fitted dipole.

Note that for 10 simulations we used in this figure three amplitudes and 10 directions for the dipoles, which means 30 dipoles per simulation. It can be seen that the clustering method seems to be closer to the input values. It should also be pointed out that one of the simulations with fixed patches seems to have difficulty in converging towards the input. It would be interesting to carry out this analysis with different patch granulometries to see whether increasing the number of patches brings us closer to the input values or not, and also perhaps to know the limit at which the number of statistics per patch is insufficient to converge. In **Fig.24** we have represented the recovered dipole by circles and the input dipole by crosses, showing the results obtained by the clustering method for the three amplitudes. One thing is clear: the higher the amplitude, the easier it is to find the input directions. However, for some directions, the amplitude is a little off. This may be due to different factors, such as the area of sky where the initial dipole is located, or to a lack of data. The black gradient represents the deviation from the input amplitude. The figure for the HEALPix method can be found in the [Appendix 4](#).

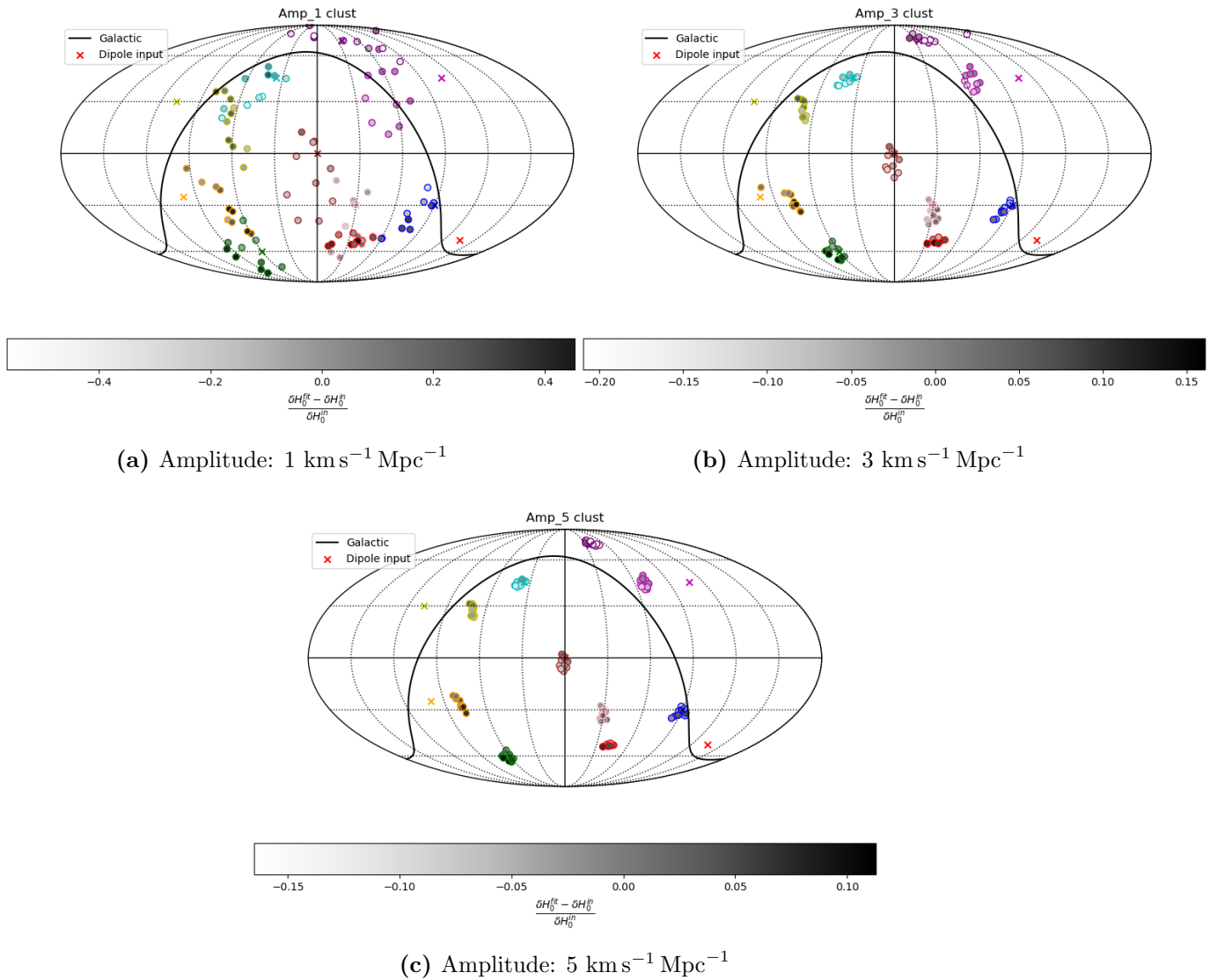


**Figure 24:** Reverse Fit for different dipoles with clustering method: (a) $1 \text{ km s}^{-1} \text{ Mpc}^{-1}$ , (b) $3 \text{ km s}^{-1} \text{ Mpc}^{-1}$ , (c) $5 \text{ km s}^{-1} \text{ Mpc}^{-1}$ . As the amplitude increases, the points cluster together.

## Conclusion

Current cosmological models, such as the  $\Lambda$ CDM, are based on the homogeneity and isotropy of the Universe. However, even if the  $\Lambda$ CDM model is the most successful to date, there are tensions in the model, such as in the Hubble constant measurements. Indeed, there is a tension of  $5\sigma$  between direct and indirect measurements. Many models attempt to correct this tension, but they are all based on the cosmological principle. Studies such as [3] point out that a dipolar cosmology shows that inclinations are not erased with cosmic acceleration.

Our subject allows us to study the anisotropy of the Hubble constant with the help of simulations of SNe Ia observed by ZTF. We demonstrate two distinct methods for partitioning the sky into different directions. The first is a fixed-patch method, while the second uses a clustering algorithm based on the distribution of SNe Ia in the sky. A first analysis of  $H_0$  variations shows that we have no anisotropies. We then introduced a dipole, as in [3]. Reiterating the analysis, we find a dipole symmetry in the variations of  $H_0$ . This analysis is therefore in line with [3]. Similarly, we find the amplitude and direction of the dipole in input. Between the two methods, we note that the clustering method is generally more efficient, but the patches will not be identical from one simulation to the next, so it's difficult to make a correct statement about its efficiency.

To take the analysis further, we need to test different patch granulometries to determine the sensitivity of the analysis. We could also redo this analysis by introducing a quadrupole, or with simulations that take into account the cosmic web which will introduce correlations in the 3D repartition of SNe Ia, as it is in real life.

## References

- [1] Jessica A. Cowell et al., “Potential signature of a quadrupolar Hubble expansion in Pantheon+ supernovae”, arXiv: <https://arxiv.org/pdf/2212.13569.pdf>, December 27, 2022
- [2] Ruairí Mc Conville and Eoin Ó Colgáin, “Anisotropic Hubble Expansion in Pantheon+ Supernovae”, arXiv: <https://arxiv.org/pdf/2304.02718.pdf>, Atlantic Technological University, Ash Lane, Sligo, Ireland, April 5, 2023
- [3] Chethan Krishnan, Ranjini Mondol and M. M. Sheikh-Jabbari, “A Tilt Instability in the Cosmological Principle”, arXiv: <https://arxiv.org/abs/2211.08093>, April 13, 2023
- [4] Melissa Amenouche, “Probing local anisotropies with Type Ia Supernovae from the Zwicky Transient Facility”, Phd thesis in Particles, Interaction and Universe, Defended on the 5<sup>th</sup> of December, 2022
- [5] Pierre-François Leget, “Modélisation des spectres des Supernovas de Type Ia observées par la collaboration The nearby Supernova Factory dans le but d'améliorer les mesures de distances extragalactiques”, HAL: <https://tel.archives-ouvertes.fr/tel-01663698>, Submitted on 14 December 2017, Defended on the 28<sup>th</sup> September 2016
- [6] NASA/WMAP Science Team, “Nine Year Microwave Sky”, black background PNG picture, <https://map.gsfc.nasa.gov/media/121238/index.html>, 04-14-2014
- [7] M.Blanton and the Sloan DIgital Sky Survey, “SDSS Galaxy Map”, JPG picture, [https://www.sdss3.org/science/gallery\\_sdss\\_pie2.php](https://www.sdss3.org/science/gallery_sdss_pie2.php), 2010-2013 SDSS-III
- [8] Ariel Goobar and Bruno Leibundgut, “Supernova Cosmology: Legacy and Future”, Annu.Rev.Nu-cl.Part.Sci 2011.61:251-79, <https://www.annualreviews.org/doi/pdf/10.1146/annurev-nucl-102010-130434>, 2011
- [9] M.Betoule et al., “Improved cosmological constraints from a joint analysis of the SDSS-II and SNLS supernova samples”, arXiv: <https://arxiv.org/abs/1401.4064>, June 4, 2014
- [10] Leandros Perivolaropoulos and Foteini Skara, “Hubble tension or a transition of the Cepheid SnIa calibrator parameters?”, arXiv: <https://arxiv.org/abs/2109.04406>, September 20, 2021
- [11] Bellm et al., “The Zwicky Transient Facility: System Overview, Performance, and First Results”, <https://iopscience.iop.org/article/10.1088/1538-3873/aaecbe/pdf>, 2019 January, Publications of the Astronomical Society of the Pacific
- [12] ZTF/Caltech, “Sky coverage”, picture comes from: [https://irsa.ipac.caltech.edu/data/ZTF/docs/releases/dr17/ztf\\_release\\_notes\\_dr17.pdf](https://irsa.ipac.caltech.edu/data/ZTF/docs/releases/dr17/ztf_release_notes_dr17.pdf)
- [13] Ulrich Feindt et al., “simsurvey: Estimationg Transient Dicover Rates for the Zwicky Transient Facility”, arXiv: <https://arxiv.org/pdf/1902.03923.pdf>, October 3, 2019
- [14] Fremling et al., “The Zwicky Transient Facility Bright Transient Survey I: Spectroscopic Classification and the Redshift Completeness of Local Galaxy Catalogs”, arXiv: <https://arxiv.org/pdf/1910.12973.pdf>, October 30, 2019
- [15] Perley et al., “The Zwicky Transient Facility Bright Transient Survey. II. A Public Statistical Sample for Exploring Supernova Demographics”, The Astrophysical Journal - The American Astronomical Society, <https://iopscience.iop.org/article/10.3847/1538-4357/abbd98/pdf>, 2020 November 20
- [16] Krysztof M. Górska et al., “The HEALPix Primer”, <http://healpix.sourceforge.io/pdf/intro.pdf>, Version 3.82, July 28, 2022

## A Appendix 1

A method that could be used, is to create our patch using the `query_polygon` routine. This query returns pixels indices on a defined polygon. So we can create for example quadrilateral and equal patches and we obtain the following map:

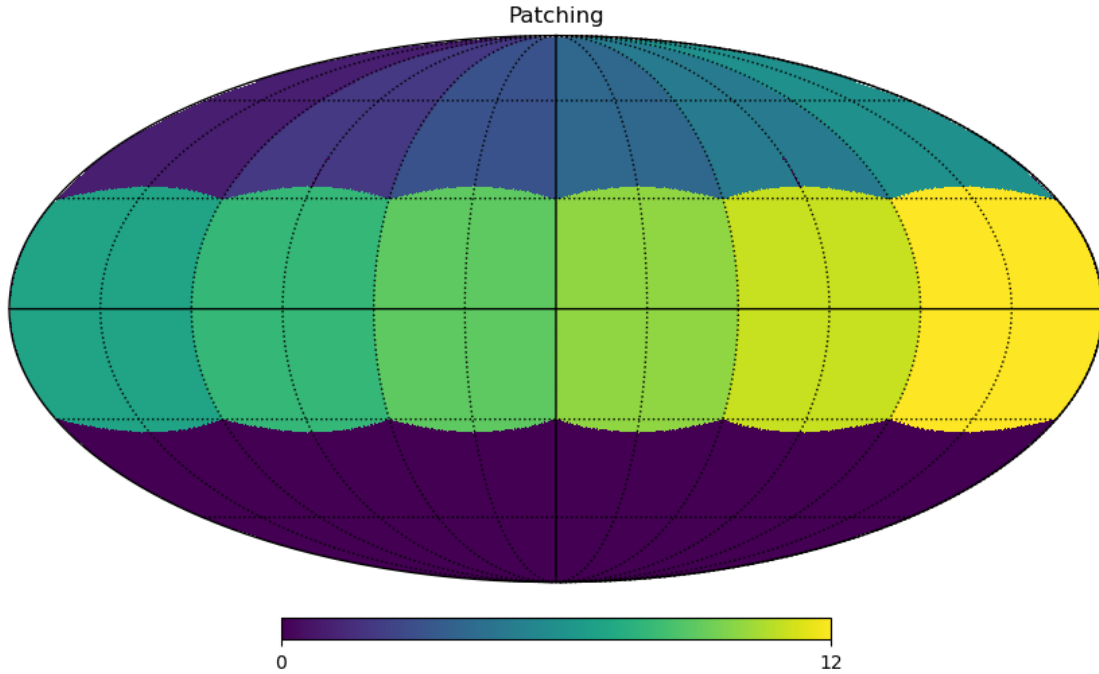


**Figure 25:** Polygon map

This method was not very efficient for our analysis due to the fact to construct patches by hand.

## B Appendix 2

Starting from the following distance modulus:

$$\mu = m - M = 5 \log D_{Mpc} + 25 \quad (.11)$$

For a source at redshift  $z$  verifying the Hubble law :

$$cz = H_0 D \quad (.12)$$

we obtain:

$$m - M = 5 \log \left( \frac{cz}{H_0} \right) + 25 \quad (.13)$$

Finally:

$$m = f(x) = 5x + b \quad (.14)$$

with

$$x = \log z \quad (.15)$$

and

$$b = 5 \log \left( \frac{c}{H_0} \right) + 25 + M \quad (.16)$$

The  $b$  parameter is function of the absolute magnitude and the Hubble constant. Therefore, if  $M$  is not constrained by other measurement, we can not determine  $H_0$  and it is why we fix  $M_B$  in our analysis. Conclusion,  $M$  and  $H_0$  are degenerated.

## C Appendix 3

Parameter	Value	Uncertainty
$\alpha$	0.1227	0.0018
$\beta$	2.970	0.018
$\delta H_0^0$	-0.34	0.21
$\delta H_0^1$	0.37	0.14
$\delta H_0^2$	-0.21	0.12
$\delta H_0^3$	-0.26	0.19
$\delta H_0^4$	0.14	0.15
$\delta H_0^5$	-0.23	0.25
$\delta H_0^6$	0.17	0.18
$\delta H_0^7$	0.45	0.25
$\delta H_0^8$	-0.4	0.4
$\delta H_0^9$	-0.1	0.7
$\delta H_0^{10}$	0.3	0.6
$\delta H_0^{11}$	-0.8	0.4

**Table 3:** Fit value for HEALPix method

Parameter	Value	Uncertainty
$\alpha$	0.1226	0.0019
$\beta$	2.971	0.019
$\delta H_0^0$	-0.26	0.21
$\delta H_0^1$	0.36	0.22
$\delta H_0^2$	-0.36	0.20
$\delta H_0^3$	-0.56	0.17
$\delta H_0^4$	0.07	0.21
$\delta H_0^5$	0.10	0.17
$\delta H_0^6$	0.05	0.20
$\delta H_0^7$	0.04	0.17
$\delta H_0^8$	0.21	0.19
$\delta H_0^9$	0.43	0.19
$\delta H_0^{10}$	-0.02	0.21

**Table 4:** Fit value for clustering method

## D Appendix 4

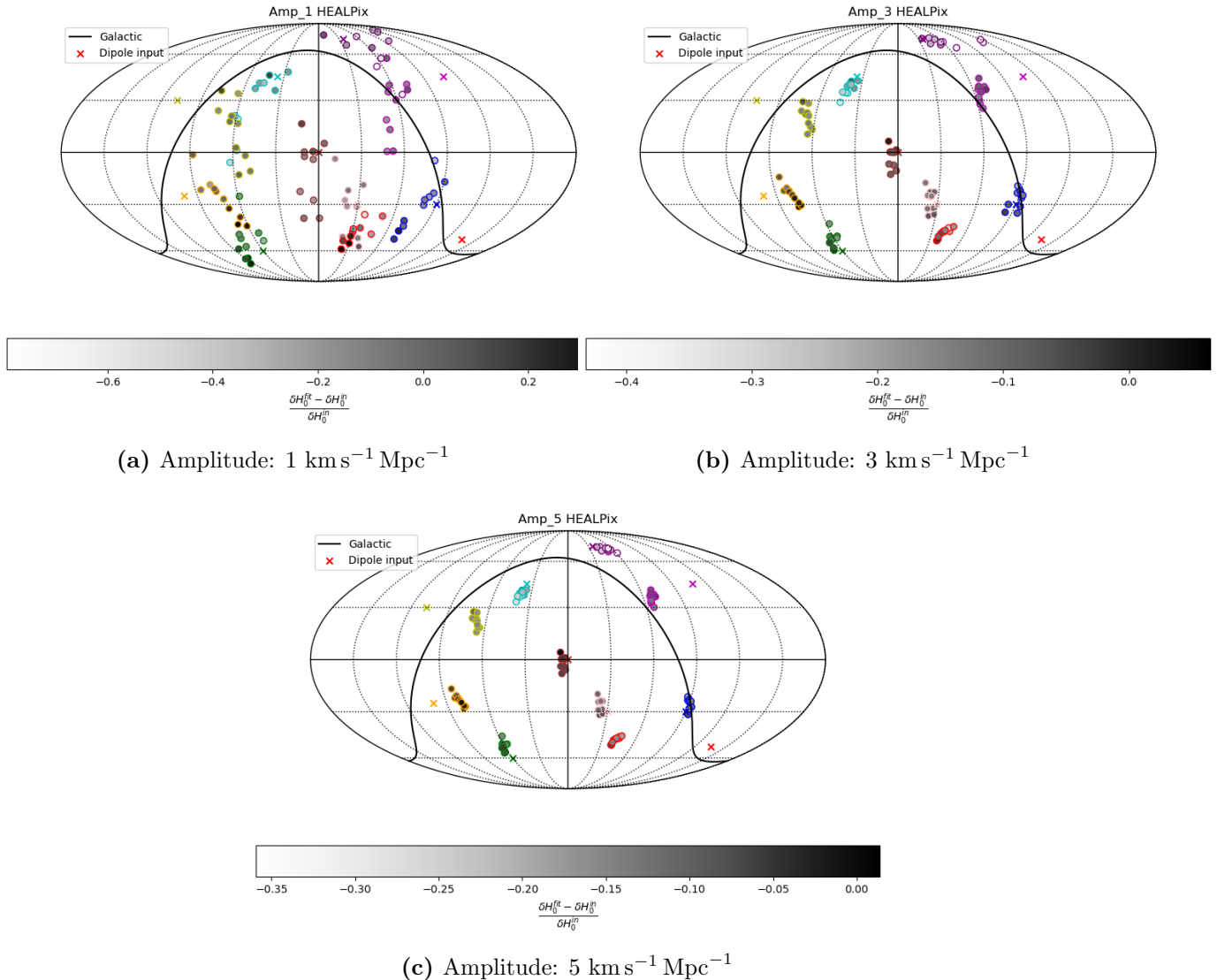


**Figure 26:** Reverse Fit for different dipoles with HEALPix method: (a) $1 \text{ km s}^{-1} \text{ Mpc}^{-1}$ , (b) $3 \text{ km s}^{-1} \text{ Mpc}^{-1}$ , (c) $5 \text{ km s}^{-1} \text{ Mpc}^{-1}$ . As the amplitude increases, the points cluster together.